UNIVERSITY OF CALIFORNIA
RIVERSIDE

Conversion of Carbon Dioxide to Formate by a Formate Dehydrogenase from *Cupriavidus necator*

A Dissertation submitted in partial satisfaction
of the requirements for the degree of

Doctor of Philosophy

in

Bioengineering

by

Xuejun Yu

September 2018

Dissertation Committee:
Dr. Ashok Mulchandani, Co-Chairperson
Dr. Xin Ge, Co-Chairperson
Dr. Russ Hille

The Dissertation of Xuejun Yu is approved:

Committee Co-Chairperson

Committee Co-Chairperson

University of California, Riverside

ACKNOWLEDGEMENTS

I would like to express sincere appreciation to my advisor, Professor Ashok Mulchandani, for accepting me to be his student when I was suffering. Thank you very much for your delicate guidance, support and encouragement during the past years. You not only guide me on my PhD study, but also help me to be mature on my personality. From bottom of my heart, I feel very lucky to have you as professor. Also, many thanks go to my other committee members. Professor Xin Ge acted as my co-advisor and provided many valuable comments on my molecular cloning work. Professor Russ Hille has also provided insights, encouragements and advices as a member of my committee members. I have learned so many important insights from our meetings and discussions and thank you for bringing me into the molybdenum/tungsten enzyme conference.

I am also thankful to the past and current group members, colleagues and friends - Dimitri Niks, Pankaj Ramnani, Feng Tan, Rabeay Hassan, Trupti Terse, Thien-Toan Tran, Claudia Chaves, Jia-wei Tay, Hui Wang, Pham Tung, Hilda Chan, Yingning Gao and Tynan Young. I had a great time working with you all, and I always feel lucky to know these wonderful people. Your friendship and support will be a wonderful memory to my PhD life. I would especially like to acknowledge the tremendous support from Dimitri Niks for valuable discussions on our collaborative projects and have helped me on many aspects.

I am grateful to the U.S. National Science Foundation for providing finding for my research. I also thank American Association for the Advancement of Science for giving me the Geraldine K. Lindsay award. This award is a great encouragement to me.

Last but surly not least, I would like to thank my parents and my husband, Haizhou Liu, for their unconditional love and support for me. My dissertation would never have been completed without encouragement from you all. You are the most important person to me. I love you all!

Part of the text of this dissertation have been published on: "Efficient reduction of CO_2 by the molybdenum-containing formate dehydrogenase from *Cupriavidus necator* (*Ralstonia eutropha*).", *J. Biol. Chem.* 2017; and "Electrochemical detection of dihydronicotinamide adenine dinucleotide using Al_2O_3-GO nanocomposite modified electrode", Arabian Journal of Chemistry 2018.

DEDICATION

To my parents and my husband

ABSTRACT OF THE DISSERTATION

Conversion of Carbon Dioxide to Formate by a Formate Dehydrogenase from *Cupriavidus necator*

by

Xuejun Yu

Doctor of Philosophy, Graduate Program in Bioengineering
University of California, Riverside, September 2018
Dr. Ashok Mulchandani, Co-Chairperson
Dr. Xin Ge, Co-Chairperson

Recently, several formate dehydrogenases have been reported to be able to catalyze the reduction of carbon dioxide to formic acid. The main challenge with these enzymes are that either the CO_2-reducing activity is very low, or highly oxygen sensitive. In this dissertation, we employed an oxygen tolerant formate dehydrogenase (FdsABG) from *Cupriavidus ncecator* (formerly known as *Ralstonia eutropha*) for conversion CO_2 to formic acid. We found that the enzyme is kinetically competent to catalyze the reverse reaction, *i.e.* reduction of CO_2 to formate by NADH, with a k_{cat} of 10 s^{-1}. Accumulation of formate in the reverse reaction was quantitatively account for consumption of NADH. It showed that all molybdenum- and tungsten-containing formate dehydrogenases, and probably also formylmethanofuran dehydrogenases, operate via a simple hydride transfer mechanism and were effective in catalyzing the reversible interconversion of CO_2 and formate. To make the reaction of CO_2 reduction more efficient and cost effective, we

cloned the full-length soluble formate dehydrogenase (FdsABG) from *C. necator* and expressed in *E. coli* with a His-tag fused to the N terminus of fdsG subunit, and this overexpression system has simplified the FdsABG purification compared to production from native *C. necator*. We further combined this engineered *C. necator* FdsABG with glucose dehydrogenase, for continuous electron donation to the reaction of converting CO_2 to formate. In dynamic electrochemistry study of FdsABG, the bioelectrocatalysis system provided electrons to FdsABG for the reduction of CO_2 to formate without the expensive reducing agent, NADH. This work provided a framework for studying the electron transfer mechanisms inside of this protein and developed a highly efficient biocatalytic process for transformation of CO_2 to formate that has applications as fuel for formic acid fuel-cells.

Table of content

List of Figures

List of Tables

Chapter 1

Introduction

1.1 Importance of CO_2 Reduction and its methods

With the ever-increasing demand of energy worldwide, the energy sector will be facing two major challenges in the near future: (1) the depleting fossil fuel reserves and (2) the excess emission greenhouse gases, especially carbon dioxide[1]. The increasing concentration of carbon dioxide (CO_2) in the atmosphere is a matter of global concern, given the serious environmental and climate implications. The major cause of increasing carbon dioxide levels in the atmosphere is the emissions from combustion of fossil fuel[2]. Hence, it is imminent to find ways to reduce atmospheric carbon dioxide levels. Currently, the most common approaches for controlling the carbon dioxide emissions that are being explored include: (1) increasing energy efficiency and conservation, (2) exploring renewable and clean energy sources such as hydrogen fuel, wind, solar, nuclear energy and biofuels, (3) capturing and sequestering carbon dioxide for other applications[3,4]. Much effort has been put into reducing carbon dioxide emissions by conservation of fossil fuel reserves and use of alternative renewable energy resources, but with the increasing global population and corresponding increase in demand for energy, the situations of depleting fossil fuel reserves and global warming have not shown much improvement. An attractive solution is the utilization of the abundantly available "waste" carbon dioxide as a feedstock

to produce useful chemicals and liquid fuels[1]. The use of carbon dioxide as a feedstock is an attractive alternative since it not only helps in reducing the atmospheric carbon dioxide level and relieve global warming, but also produces renewable clean energy and useful chemicals to combat the energy crisis. However, these processes remain challenging in both industry and nature[1,3,5].

For conversion of carbon dioxide to liquid fuels and chemicals, different methods such as heterogeneous catalysis, electrocatalysis and photocatalysis have been used in the industry. However, the shortcomings of these methods are: (1) requirement of hydrogen, (2) high-temperature and high-pressure reaction condition, and (3) low selectivity and yield [6,7]. In comparison to these shortcomings, reduction of CO_2 using biocatalysts is an attractive alternative as it requires mild conditions and offers higher selectivity and yield.

1.2 Biological systems are widely applied in carbon dioxide fixation process

In nature, carbon dioxide fixation is not a novelty. For example, most plants, algae, and cyanobacteria can utilize carbon dioxide for photosynthesis. Additionally, some microorganisms can perform chemosynthesis to fix carbon dioxide. Also, this naturally occurring process of fixing carbon dioxide happens on a very large scale. On average, about 385 Giga tons of carbon dioxide is fixed through photosynthesis process every year 8. However, most of the products from these naturally occurring processes include carbohydrates and proteins, which cannot be utilized as high energy density fuels. The resulting carbohydrates can in turn be converted to high energy density fuels by methods

such as fermentation, metabolic engineering and biofuel cells. In comparison, direct conversion of CO_2 to liquid fuel through biological method is a more attractive option[1].

Another emerging area of study, enzymatic bioelectrocatalysis, have brought great attention and increasingly studies [9-14]. The difference between biocatalysis and enzymatic bioelectrocatalysis is the difference of electron source. Figure 1.1 are schematics of converting CO_2 to formate through biocataysis and bioelectrocatalysis, which were modified from Milton *et. al.* for summarizing the difference[13]. Biocatalysis (Figure 1.1A) reactions is always a redox reaction and catalyzed by biological enzymes, and such redox reaction involves an electron(s) and coupled with electron transfer associate with those oxidoreductases[13]. Enzymatic cofactors such as NAD(P)H donate electrons to the oxidoreductase, and oxidoreductase passes the electrons to the substrate of CO_2. While in bioelectrocatalysis (Figure 1.1B and Figure 1.1C), the electrons can communicate with adsorbed enzyme through a small electron mediator (Figure 1.1B), or direct communicate with the electrode (Figure 1.1C) [13]. Enzymatic bioelectrocatalysis not only have taken the advantages from biocatalysis, such as mild reaction condition and specific substrate, but also bypass the expensive electron cofactors. Dynamic electrochemical studies of adsorbed enzymes on electrodes not only provide the electrons of the redox reaction, but also introduce the "potential dimension" into the enzyme kinetics and biocatalysis reaction[15]. Another advantage of bioelectrocatalysis is making the redox reaction with higher reaction rate and efficiency compared with biocatalysis[14]. Dynamic bioelectrochemistry studies not

only provide better understand on enzyme, but also provide fundamental techniques for biofuel cells and biosensors[13].

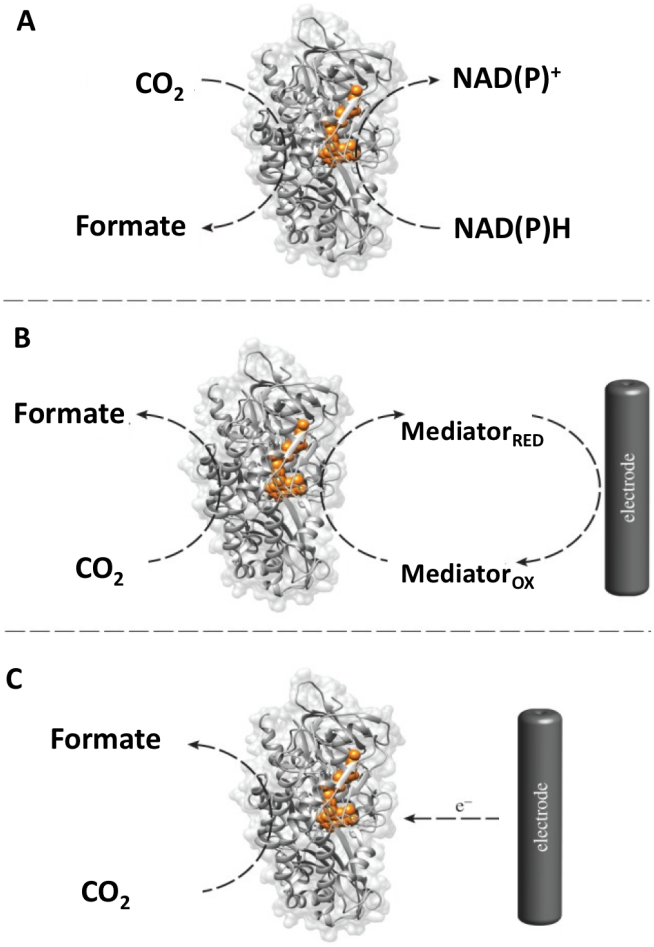

Figure 1.1 *Schematics of converting CO_2 to formate through (A) biocataysis by an enzyme (B) mediated electron transfer type bioelectrocatalysis and (C) direct electron transfer type bioelectrocatalysis.*[13]

Recent years, formic acid has become a promising liquid fuel, a hydrogen energy carrier with advantages of high volumetric capacity (53 g H_2/L), low toxicity and flammability under ambient conditions, as well as an important feedstock for synthesis of other valuable chemicals[3,16-18]. In comparison, biocatalysts for the conversion of CO_2 to liquid fuel have the advantages of mild reaction conditions: room temperature under ambient pressure, and neutral pH[19]. Thus, direct conversion of CO_2 to useful chemicals/liquid fuels, such as formic acid, through biological enzyme is a more attractive option. Several formate dehydrogenases (FDHs) have been reported to be able to convert CO_2 to formic acid, but these enzymes remain challenging due to low reaction efficiency and enzyme oxygen sensitivity[20].

1.3 Formate Dehydrogenase

Formate dehydrogenases (FDHs) are a heterogeneous group of enzymes that are widely found in a variety of organisms that include anaerobic bacteria, aerobic bacteria, archaea, yeasts, fungi and plants[21]. All FDHs catalyze the oxidation reaction of formic acid to carbon dioxide, generating two protons and two electrons (Equation 1.1).

$$HCOOH \xrightarrow{FDH} CO_2 + 2H^+ + 2e^- \qquad \text{(Eq. 1.1)}$$

FDHs can be broadly classified into three categories: metal-independent/NAD(P)$^+$-dependent FDHs, metal-containing/NAD(P)$^+$-independent FDHs, and metal-containing/NAD(P)$^+$-dependent FDHs[20]. Take NAD(P)$^+$-dependent FDHs as an example, the electrons and protons generated by FDHs reaction transform NAD(P)$^+$ to NAD(P)H. Subsequently, NAD(P)H flows to the electron transport chain and produces a source of energy for cell biosynthetic and metabolism. Thus, FDHs play a significant role in a wide variety of fermentation pathways as well as respiration pathways[21]. Studies have shown the utilization of FDHs for NAD(P)H cofactor regeneration in vitro[22]. Further in a recent 2012 study, Li et al. utilized membrane bound FDHs to generate NADH by feeding cells with formic acid, and the NADH generated provided reducing power for metabolic pathways of producing biofuels such as isobutanol and 3-methyl-1-butanol[10]. Recently, several FDHs have been reported to be able to catalyze the reverse reaction, which is the reduction of carbon dioxide to formic acid under appropriate conditions (Equation 1.2).

$$CO_2 + 2H^+ + 2e^- \xrightarrow{FDH} HCOOH \qquad \text{(Eq. 1.2)}$$

Formate dehydrogenase from yeast *Candida boidinii* (CbFDH) and formate dehydrogenase from bacteria *Thiobacillus sp.* KNK65MA (TsFDH) are two examples of metal-independent/NAD(P)$^+$-dependent FDHs. CbFDH, in particular, has been widely investigated for reduction of CO_2 in various forms, (e.g. enzymatic, electrochemical, and photochemical reaction) [23-27].

1.4 Challenges of enzymatic CO_2 reduction

The problem with these enzymes is that the CO_2-reducing activity is very low. For example, k_{cat} for TsFDH was reported as 0.318 s^{-1} and k_{cat} for CbFDH was reported to be 0.015 s^{-1} [27]. In comparison, the metal-dependent/$NAD(P)^+$-independent FDHs contain tungsten or molybdenum in their active site and have a high CO_2-reducing activity. For example, *S. fumaroxidans* FDH1 and *S. fumaroxidans* FDH2 were as reported to have an extremely high CO_2-reducing activity with k_{cat} about 2.5 x 10^3 s^{-1} and 0.2 x 10^3 s^{-1}, respectively [28]. However, these enzymes are extremely oxygen sensitive because of the presence of selenocysteine at the tungsten active site, rendering them unsuitable for industrial applications.

In 2013, a new molybdenum-dependent/NAD^+-dependent FDH from bacteria *Rhodobacter capsulatus* was reported to be oxygen-tolerant [29]. Also, a similar soluble molybdenum-dependent/NAD^+-dependent FDH (FdsABG) from *Cupriavidus necator* (formerly known as *Ralstonia eutropha*) has successfully purified by Niks *et al* [30]. This soluble FdsABG was found to be oxygen-tolerant and based on our results (chapter 2), the native FdsABG purified from *C. nector* is in fact effectively catalyze the reduction of CO_2 using NADH as a terminal electron donor with k_{cat} of 10 s^{-1} to native FdsABG, or 5 s^{-1} to recombinant FdsABG [31]. Table 1.1 summarizes the feature and the $k_{cat}^{CO_2}$ of some FDHs. Although some FDHs have high catalytic activities of CO_2 reduction, they also have many thorny problems for practical applications, including oxygen sensitivity and difficult to

purify. In comparison of all FDHs, FdsABG from *C. nector* has both advantages of O_2 tolerance and high activity of CO_2 reduction.

Table 1.1 List of formate dehydrogenases and their properties

Enzyme Source	Metal dependence	k_{cat} (1/s) *	O_2 sensitivity	Ref
C. boidinii	No	0.015	-	27
Thiobacillus sp. KNK65MA	No	0.318	-	27
S. fumaroxidans, FDH1	Tungsten (W)	2500	+++	28
S. fumaroxidans, FDH2	Tungsten (W)	200	+++	28
Clostridium carboxidivorans	Tungsten (W)	0.08	+++	32
E. coli	Molybdenum (Mo)	<1	+++	9
Desulfovibrio desulfuricans	Molybdenum (Mo)	46.6	+++	33
Acetobacterium woodii	Molybdenum (Mo)	28	+++	34
R. capsulatus	Molybdenum (Mo)	1.5	+	29
Cupriavidus necator FdsABG	Molybdenum (Mo)	10	+	31

Note: k_{cat} values are for CO_2 reduction reactions.

1.5 Scope of this thesis

The overall objective of this Ph.D. thesis is to investigate a high-efficiency and cost-effective process for transformation of the waste greenhouse gas carbon dioxide into a useful chemical fuel, formic acid, by using this novel high CO_2-reducing activity and oxygen tolerant formate dehydrogenase (FdsABG) from *Cupriavidus necator* (formerly known as *Ralstonia eutropha*).

Objectives: (1) Optimize the CO_2-reduction reaction conditions using novel soluble formate dehydrogenase from *Cupriavidus necator* (FdsABG). (2) Achieve FdsABG recombinant production and continuous CO_2 to formate conversion. (3) Study the dynamic electrochemistry of the recombinant FdsABG with adsorbed on electrodes.

1.5.1 Chapter 2: Efficient reduction of CO_2 by FdsABG from *Cupriavidus necator* (*Ralstonia eutropha*).

Cupriavidus necator is an aerobic facultative chemoautotroph bacterium, and this organism is capable of growing both heterotrophically and lithoautotrophically [35]. The *C. necator* genome encodes four formate dehydrogenases; three of them are membrane bound and one is the soluble molybdenum-dependent/NAD^+-dependent FDH (FdsABG) found in the cytoplasm [36]. FdsABG belongs to the DMSO reductase family of Mo and W enzymes, and is a soluble homodimer complex of trimers, *i.e.*, $(\alpha\beta\gamma)_2$, containing one molybdenum active center, one FMN and seven Fe/S centers [37,38]. The α subunit (*fdsA*) contains the molybdenum active center and five Fe/S centers, and this α subunit is responsible for binding formic acid and carbon dioxide [38]. The ß subunit (*fdsB*) contains one FMN and one Fe/S center. The ß subunit is responsible for NAD^+ reduction. The γ subunit (*fdsG*) contains one Fe/S center, and both ß and γ subunits form an active diaphorase unit [38]. Currently, the FdsABG 3D structure is unknown. Figure 1.2 shows the FdsABG protein architecture model and the schematic of the reduction of CO_2 to formic acid catalyzed by FdsABG with requirement of NADH, as proposed in review paper[37].

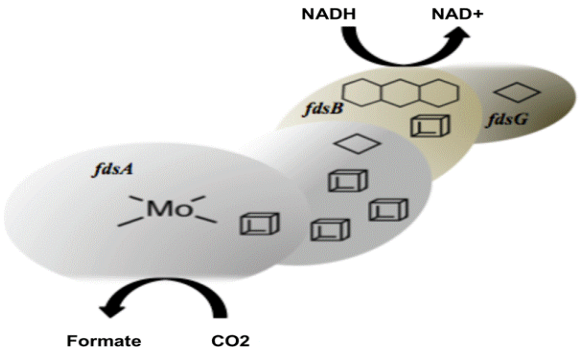

Figure 1.2 *Protein architecture model of C. necator FdsABG*[37]

FdsABG has only been successfully purified from *Cupriavidus necator* H16 and *C. necator* HF210 [35], a streptomycin-resistant mutant strain derived from wild-type *C. necator* H16 strain. However, culturing process of *C. necator* is very complex and time-consuming, which contains about 4 days of pre-culture, 6 hours of mass culture, and followed by 2 days of fermentation [35]. Additionally, the FdsABG purification process is also very complex, time-consuming and expensive. The purification process requires two ammonium sulfate cuts and five different FPLC affinity columns [35].

In this study, we will study the optimum condition of the FdsABG purified from *C. necator* for catalyzing CO_2 to formate, the enzyme steady-state kinetic. Beyond on the studies of FdsABG, we have also found a problem of using bicarbonate as a substrate for the reaction of CO_2 reduction. Once bicarbonate dissolve in solution, the bicarbonate will have an equilibrium between the dissolved CO_2 and the other two species, carbonic acid and carbonate. The equilibrium process will not only happen within the solution, but also at the headspace of solution. If the bicarbonate solution expose to an open space, the dissolved CO_2 in solution will continues release to the air, and thus the CO_2 concentration in solution will drop continuously. Figure 1.3 demonstrate this equilibrium process.

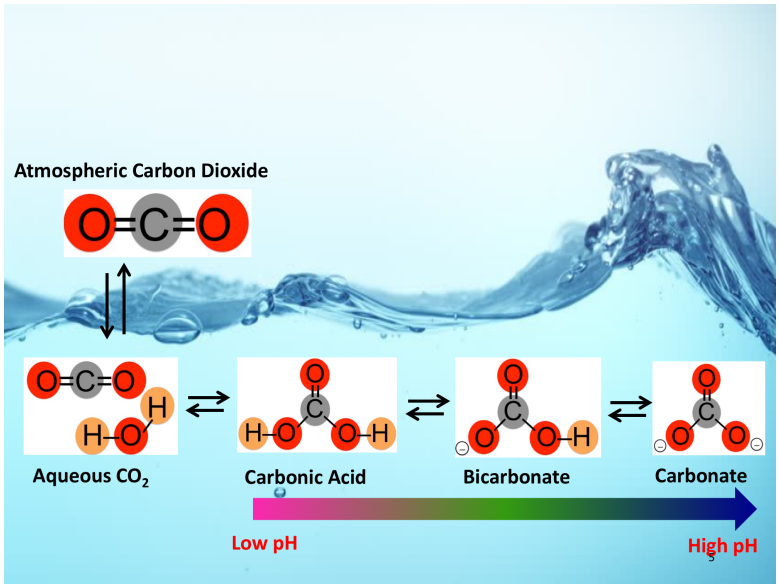

Figure 1.3. *Equilibrium between bicarbonate, carbonic acid, carbonate, and aqueous* CO_2

1.5.2 Chapter 3: Synthesis of Formate from CO_2 Gas Catalyzed by fdsABG and Glucose Dehydrogenase

As mentioned above, the current process of purifying a small quantity of FdsABG is highly time consuming and complex. Therefore, efficient production of FdsABG is important for improving the reaction process of reducing CO_2 to formic acid cost and time efficient. For current research, FDH from *Rhodobacter capsulatus* (RcFDH), which shows similar protein structure properties to FdsABG, has been successfully cloned and express in *E. coli* [29]. In this study, we will clone the full-length soluble formate dehydrogenase (FdsABG) from *C. necator* and expressed in *E. coli* with a His-tag fused to the with the N terminus of fdsG subunit. Our ultimate goal is that this overexpression system will simplify

the FdsABG culture process and purification process compared with native bacteria *C. necator*.

Moreover, the reaction of reducing CO_2 to formic acid catalyzed by FdsABG requires NADH to provide sufficient energy. However, NADH is very expensive (~$1000/mol) and is consumed in stoichiometric quantity, regeneration of nicotinamide cofactor is essential for the reaction to be cost-effective. At the same time, regenerating NADH from NAD^+ will also help drive the thermodynamically unfavorable reaction towards product formation, thereby improving reaction yield [22]. Therefore, efficient regeneration of NADH cofactor is important for improving the reaction yield of reducing CO_2 to formic acid. As previously reported, NADH has been successfully regenerated from NAD^+ by enzymatic, photocatalytic and electrochemical methods[10,22,24,39]. In this study, we will also combine this engineered *C. necator* FdsABG with another biological enzyme, Glucose Dehydrogenase, for continuous electrons donation to the reaction of converting CO_2 to formate.

1.5.3 Chapter 4: Electrochemistry Study of FdsABG from *Cupriavidus necator*

As mentioned above, dynamic electrochemical studies of adsorbed enzymes on electrodes not only provide the electrons of the redox reaction, but also introduce the "potential dimension" into the enzyme kinetics and biocatalysis reaction[15]. Many metal-containing enzymes have been studied on electrodes, and have been applied to other fields of studies, such as biosensor and biofuel cells[13]. Only several FDHs were studied on electrode, including the W-dependent FDH from *Syntrophobacter fumaroxidans* (*Sf*FDH1)

[12], Mo-dependent FDH from *E. coli* (*Ec*FDH-H) [9] and the yeast FDH from *Candida boidinii* (CbFDH) [25,40]. For CbFDH, researches have been combined this enzyme with electrochemical reduction of NADH for effectively reduction of CO_2 [40]. *Sf*FDH1 and *Ec*FDH-H are the only two FDHs that have studied on electrode for bioelectrocatalysis through direct electron transfer (DET) process. In this objective, we will apply FdsABG on different electrodes and study the dynamic electrochemistry of the enzyme. Direct electron transfer is the most anticipated process, and mediated electron transfer process will also be studied.

1.6 Reference

1. Aresta, M.; Dibenedetto, A., Utilization of CO_2 as a chemical feedstock: opportunities and challenges. Dalton Transactions 2007, (28), 2975-2992.

2. Aresta, M.; Dibenedetto, A.; Angelini, A., Catalysis for the Valorization of Exhaust Carbon: from CO_2 to Chemicals, Materials, and Fuels. Technological Use of CO_2. Chemical Reviews 2014, 114 (3), 1709-1742.

3. Appel, A. M.; Bercaw, J. E.; Bocarsly, A. B.; Dobbek, H.; DuBois, D. L.; Dupuis, M.; Ferry, J. G.; Fujita, E.; Hille, R.; Kenis, P. J. A.; Kerfeld, C. A.; Morris, R. H.; Peden, C. H. F.; Portis, A. R.; Ragsdale, S. W.; Rauchfuss, T. B.; Reek, J. N. H.; Seefeldt, L. C.; Thauer, R. K.; Waldrop, G. L., Frontiers, Opportunities, and Challenges in Biochemical and Chemical Catalysis of CO_2 Fixation. Chemical Reviews 2013, 113 (8), 6621-6658.

4. Zhang, W. J.; Hu, Y.; Ma, L. B.; Zhu, G. Y.; Wang, Y. R.; Xue, X. L.; Chen, R. P.; Yang, S. Y.; Jin, Z., Progress and Perspective of Electrocatalytic CO_2 Reduction for Renewable Carbonaceous Fuels and Chemicals. Advanced Science 2018, 5 (1).

5. Boot-Handford, M. E.; Abanades, J. C.; Anthony, E. J.; Blunt, M. J.; Brandani, S.; Mac Dowell, N.; Fernandez, J. R.; Ferrari, M. C.; Gross, R.; Hallett, J. P.; Haszeldine, R. S.; Heptonstall, P.; Lyngfelt, A.; Makuch, Z.; Mangano, E.; Porter, R. T. J.; Pourkashanian, M.; Rochelle, G. T.; Shah, N.; Yao, J. G.; Fennell, P. S., Carbon capture and storage update. Energy & Environmental Science 2014, 7 (1), 130-189.

6. Sun, Q.; Jiang, Y.; Jiang, Z.; Zhang, L.; Sun, X.; Li, J., Green and Efficient Conversion of CO_2 to Methanol by Biomimetic Coimmobilization of Three Dehydrogenases in Protamine-Templated Titania. Industrial & Engineering Chemistry Research 2009, 48 (9), 4210-4215.

7. Olah, G. A., Beyond oil and gas: The methanol economy. Angewandte Chemie-International Edition 2005, 44 (18), 2636-2639.

8. Geider, R. J.; Delucia, E. H.; Falkowski, P. G.; Finzi, A. C.; Grime, J. P.; Grace, J.; Kana, T. M.; La Roche, J.; Long, S. P.; Osborne, B. A.; Platt, T.; Prentice, I. C.; Raven, J. A.; Schlesinger, W. H.; Smetacek, V.; Stuart, V.; Sathyendranath, S.; Thomas, R. B.; Vogelmann, T. C.; Williams, P.; Woodward, F. I., Primary productivity of planet earth: biological determinants and physical constraints in terrestrial and aquatic habitats. Global Change Biology 2001, 7 (8), 849-882.

9. Bassegoda, A.; Madden, C.; Wakerley, D. W.; Reisner, E.; Hirst, J., Reversible lnterconversion of CO_2 and Formate by a Molybdenum-Containing Formate Dehydrogenase. Journal of the American Chemical Society 2014, 136 (44), 15473-15476.

10. Li, H.; Opgenorth, P. H.; Wernick, D. G.; Rogers, S.; Wu, T.-Y.; Higashide, W.; Malati, P.; Huo, Y.-X.; Cho, K. M.; Liao, J. C., Integrated Electromicrobial Conversion of CO_2 to Higher Alcohols. Science 2012, 335 (6076), 1596-1596.

11. Li, H.; Liao, J. C., Biological conversion of carbon dioxide to photosynthetic fuels and electrofuels. Energy & Environmental Science 2013, 6 (10), 2892-2899.

12. Reda, T.; Plugge, C. M.; Abram, N. J.; Hirst, J., Reversible interconversion of carbon dioxide and formate by an electroactive enzyme. Proceedings of the National Academy of Sciences of the United States of America 2008, 105 (31), 10654-10658.

13. Milton, R. D.; Minteer, S. D., Direct enzymatic bioelectrocatalysis: differentiating between myth and reality. Journal of the Royal Society Interface 2017, 14 (131), 13.

14. Armstrong, F. A.; Hirst, J., Reversibility and efficiency in electrocatalytic energy conversion and lessons from enzymes. Proceedings of the National Academy of Sciences of the United States of America 2011, 108 (34), 14049-14054.

15. Armstrong, F. A., Recent developments in dynamic electrochemical studies of adsorbed enzymes and their active sites. Current Opinion in Chemical Biology 2005, 9 (2), 110-117.

16. Enthaler, S.; von Langermann, J.; Schmidt, T., Carbon dioxide and formic acid-the couple for environmental-friendly hydrogen storage? Energy & Environmental Science 2010, 3 (9), 1207-1217.

17. Sordakis, K.; Tang, C. H.; Vogt, L. K.; Junge, H.; Dyson, P. J.; Beller, M.; Laurenczy, G., Homogeneous Catalysis for Sustainable Hydrogen Storage in Formic Acid and Alcohols. Chemical Reviews 2018, 118 (2), 372-433.

18. Yadav, M.; Xu, Q., Liquid-phase chemical hydrogen storage materials. Energy & Environmental Science 2012, 5 (12), 9698-9725.

19. Shi, J. F.; Jiang, Y. J.; Jiang, Z. Y.; Wang, X. Y.; Wang, X. L.; Zhang, S. H.; Han, P. P.; Yang, C., Enzymatic conversion of carbon dioxide. Chemical Society Reviews 2015, 44 (17), 5981-6000.

20. Maia, L. B.; Moura, I.; Moura, J. J. G., Molybdenum and tungsten-containing formate dehydrogenases: Aiming to inspire a catalyst for carbon dioxide utilization. Inorganica Chimica Acta 2017, 455, 350-363.

21. Maia, L. B.; Moura, J. J. G.; Moura, I., Molybdenum and tungsten-dependent formate dehydrogenases. Journal of Biological Inorganic Chemistry 2015, 20 (2), 287-309.

22. Weckbecker, A.; Groeger, H.; Hummel, W., Regeneration of Nicotinamide Coenzymes: Principles and Applications for the Synthesis of Chiral Compounds. Biosystems Engineering, I: Creating Superior Biocatalysts 2010, 120, 195-242.

23. El-Zahab, B.; Donnelly, D.; Wang, P., Particle-tethered NADH for production of methanol from CO_2 catalyzed by coimmobilized enzymes. Biotechnology and Bioengineering 2008, 99 (3), 508-514.

24. Yadav, R. K.; Baeg, J.-O.; Oh, G. H.; Park, N.-J.; Kong, K.-j.; Kim, J.; Hwang, D. W.; Biswas, S. K., A Photocatalyst-Enzyme Coupled Artificial Photosynthesis System for Solar Energy in Production of Formic Acid from CO_2. Journal of the American Chemical Society 2012, 134 (28), 11455-11461.

25. Kim, S.; Kim, M. K.; Lee, S. H.; Yoon, S.; Jung, K.-D., Conversion of CO_2 to formate in an electroenzymatic cell using *Candida boidinii* formate dehydrogenase. Journal of Molecular Catalysis B-Enzymatic 2014, 102, 9-15.

26. Srikanth, S.; Maesen, M.; Dominguez-Benetton, X.; Vanbroekhoven, K.; Pant, D., Enzymatic electrosynthesis of formate through CO_2 sequestration/reduction in a bioelectrochemical system (BES). Bioresource Technology 2014, 165, 350-354.

27. Choe, H.; Joo, J. C.; Cho, D. H.; Kim, M. H.; Lee, S. H.; Jung, K. D.; Kim, Y. H., Efficient CO_2-Reducing Activity of NAD-Dependent Formate Dehydrogenase from *Thiobacillus sp* KNK65MA for Formate Production from CO_2 Gas. Plos One 2014, 9 (7).

28. de Bok, F. A. M.; Hagedoorn, P. L.; Silva, P. J.; Hagen, W. R.; Schiltz, E.; Fritsche, K.; Stams, A. J. M., Two W-containing formate dehydrogenases (CO_2-reductases) involved in syntrophic propionate oxidation by *Syntrophobacter fumaroxidans*. European Journal of Biochemistry 2003, 270 (11), 2476-2485.

29. Hartmann, T.; Leimkuehler, S., The oxygen-tolerant and NAD($^+$)-dependent formate dehydrogenase from Rhodobacter capsulatus is able to catalyze the reduction of CO_2 to formate. Febs Journal 2013, 280 (23), 6083-6096.

30. Niks, D.; Duvvuru, J.; Escalona, M.; Hille, R., Spectroscopic and Kinetic Properties of the Molybdenum-containing, NAD(+) - dependent Formate Dehydrogenase from *Ralstonia eutropha*. Journal of Biological Chemistry 2016, 291 (3), 1162-1174.

31. Yu, X. J.; Niks, D.; Mulchandani, A.; Hille, R., Efficient reduction of CO_2 by the molybdenum-containing formate dehydrogenase from *Cupriavidus necator* (*Ralstonia eutropha*). Journal of Biological Chemistry 2017, 292 (41), 16872-16879.

32. Alissandratos, A.; Kim, H.-K.; Matthews, H.; Hennessy, J. E.; Philbrook, A.; Easton, C. J., *Clostridium carboxidivorans* Strain P7T Recombinant Formate Dehydrogenase Catalyzes Reduction of CO_2 to Formate. Applied and Environmental Microbiology 2013, 79 (2), 741-744.

33. Maia, L. B.; Fonseca, L.; Moura, I.; Moura, J. J. G., Reduction of Carbon Dioxide by a Molybdenum-Containing Formate Dehydrogenase: A Kinetic and Mechanistic Study. Journal of the American Chemical Society 2016, 138 (28), 8834-8846.

34. Schuchmann, K.; Mueller, V., Direct and Reversible Hydrogenation of CO_2 to Formate by a Bacterial Carbon Dioxide Reductase. Science 2013, 342 (6164), 1382-1385.

35. Friedebold, J.; Bowien, B., Physiological and biochemical characterization of the soluble formate dehydrogenase, a molybdoenzyme from *Alcaligenes eutrophus*. Journal of Bacteriology 1993, 175 (15), 4719-4728.

36. Pohlmann, A.; Fricke, W. F.; Reinecke, F.; Kusian, B.; Liesegang, H.; Cramm, R.; Eitinger, T.; Ewering, C.; Potter, M.; Schwartz, E.; Strittmatter, A.; Voss, I.; Gottschalk, G.; Steinbuchel, A.; Friedrich, B.; Bowien, B., Genome sequence of the bioplastic-producing "Knallgas" bacterium *Ralstonia eutropha* H16. Nature Biotechnology 2006, 24 (10), 1257-1262.

37. Hille, R.; Hall, J.; Basu, P., The Mononuclear Molybdenum Enzymes. Chemical Reviews 2014, 114 (7), 3963-4038.

38. Oh, J. I.; Bowien, B., Structural analysis of the fds operon encoding the NAD(+)-linked formate dehydrogenase of *Ralstonia eutropha*. Journal of Biological Chemistry 1998, 273 (41), 26349-26360.

39. Aresta, M.; Dibenedetto, A.; Baran, T.; Angelini, A.; Labuz, P.; Macyk, W., An integrated photocatalytic/enzymatic system for the reduction of CO_2 to methanol in bioglycerol-water. Beilstein Journal of Organic Chemistry 2014, 10, 2556-2565.

40. Addo, P. K.; Arechederra, R. L.; Waheed, A.; Shoemaker, J. D.; Sly, W. S.; Minteer, S. D., Methanol Production via Bioelectrocatalytic Reduction of Carbon Dioxide: Role of Carbonic Anhydrase in Improving Electrode Performance. Electrochemical and Solid State Letters 2011, 14 (4), E9-E13.

Chapter 2

Efficient reduction of CO_2 by the molybdenum-containing formate dehydrogenase from *Cupriavidus necator* (*Ralstonia eutropha*).

This chapter is based on Yu, X. *et al.* (2017) *Journal of Biological Chemistry* 292, 16872-16879

2.1 Abstract

The ability of the FdsABG formate dehydrogenase from *Cupriavidus necator* (formerly known as *Ralstonia eutropha*) to catalyze the reverse of the physiological reaction, the reduction of CO_2 to formate utilizing NADH as electron donor, has been investigated. Contrary to previous studies of this enzyme, we demonstrate that it is in fact effective in catalyzing the reverse reaction, with a k_{cat} of 10 s^{-1}. We also quantify the stoichiometric accumulation of formic acid as the product of the reaction and demonstrate that the observed kinetic parameters for catalysis in the forward and reverse reaction are thermodynamically consistent, complying with the expected Haldane relationships. Finally, we demonstrate the reaction conditions necessary for gauging the ability of a given formate dehydrogenase or other CO_2-utilizing enzyme to catalyze the reverse direction so as to avoid false negative results. In conjunction with our earlier studies on the reaction mechanism of this enzyme (Niks *et al.* (2016) *J. Biol. Chem.* **291**, 1162-1174), and on the basis of the present work we conclude that all molybdenum- and tungsten-containing

formate dehydrogenases and related enzymes likely operate via a simple hydride transfer mechanism and are effective in catalyzing the reversible interconversion of CO_2 and formate under the appropriate experimental conditions.

2.2 Introduction

Formate dehydrogenases are a heterogeneous group of enzymes that are widely distributed in biology, being found in anaerobic as well as aerobic bacteria, archaea, yeasts, fungi, plants and vertebrates. These enzymes can be broadly classified as metal-independent/NAD(P)$^+$-dependent, metal-containing/NAD(P)$^+$-dependent, and metal-containing/NAD(P)$^+$-independent[1]. All these enzymes catalyze the oxidation of formic acid to carbon dioxide, generating two protons and two electrons (Equation 2.1):

$$HCOOH \longrightarrow CO_2 + 2H^+ + 2e^- \qquad \text{(Eq. 2.1)}$$

Some, but not all, metal-containing formate dehydrogenases have been reported to catalyze the reverse reaction, *i.e.*, the reduction of carbon dioxide to formic acid, a reaction of considerable industrial interest given the general difficulty of activating CO_2 for reduction[1-4]. The main challenges in the use of these enzymes for the generation of formate are the low rates of CO_2-reducing activity typically reported and the high O_2-sensitivity exhibited by most of these enzymes[5]. In the present study, we have examined the ability of an oxygen-tolerant formate dehydrogenase from *Cupriavidus necator* (FdsABG) to convert CO_2 to formic acid.

Cupriavidus necator (formerly known as *Ralstonia eutropha*) is an aerobic facultative chemoautotrophic bacterium capable of both heterotrophic and lithoautotrophic growth[6]. The *C. necator* genome encodes four formate dehydrogenases, all of which are metal-dependent. Three are membrane-bound and expressed under various growth conditions, while one is cytoplasmic. This last enzyme, encoded by the *fdsGBACD* operon and consisting of the FdsABG gene products[7], is an O_2-tolerant homodimer of trimers, $(\alpha\beta\gamma)_2$[8, 9]. The 105 kDa α-subunit (FdsA) contains the molybdenum-containing active site, as well as four [4Fe-4S] clusters and a [2Fe-2S] cluster. Oxidation of formic acid occurs at the molybdenum center, which in the oxidized enzyme has an $L_2Mo^{VI}S$(S-Cys) structure (L representing the pyranopterin cofactor found in all molybdenum- and tungsten-containing enzymes other than nitrogenase, a guanine dinucleotide in the present case); reduction yields an L_2Mo^{IV}(SH)(S-Cys) center[9]. The 55 kDa β-subunit (FdsB) contains FMN and a [4Fe-4S] cluster, with the FMN being the site of NAD^+ reduction. Finally, the 19 kDa γ-subunit (FdsG) contains one [2Fe-2S] cluster. The three subunits of the *C. necator* FdsABG formate dehydrogenase have strong sequence homology to the corresponding Nqo3, Nqo1 and Nqo2 subunits, respectively, of the crystallographically characterized *Thermus thermophilus* NADH dehydrogenase[10], and the enzyme thus belongs to the NADH dehydrogenase superfamily of enzymes. The enzyme is unusual among the metal-dependent formate dehydrogenases in being O_2-tolerant, and unusual among the NADH dehydrogenases in being cytosolic (and water-soluble) rather than membrane-integral. The large number of iron-sulfur clusters as well as the FMN are unique

among the formate dehydrogenases and possibly afford a greater number of potential pathways for electrochemical reduction.

In previous work, we have characterized the rapid reaction kinetics and spectroscopic properties of *C. necator* FdsABG and demonstrated that the enzyme operates via a ping-pong mechanism with a limiting rate constant, k_{red}, for reduction of enzyme by formate of 140 s^{-1} at 10˚C (corresponding to 560 s^{-1} at 30˚C) and a K_d of 82 μM[11]. We have also characterized the EPR signal of the molybdenum center in its Mo^V state and demonstrated the direct transfer of the substrate C_α hydrogen to the molybdenum center in the course of the reaction, concluding that the reaction proceeds via direct hydride transfer from substrate to the Mo=S group of the active site molybdenum center, with CO_2 (rather than bicarbonate) as the immediate product of the overall reaction (Figure 2.1).

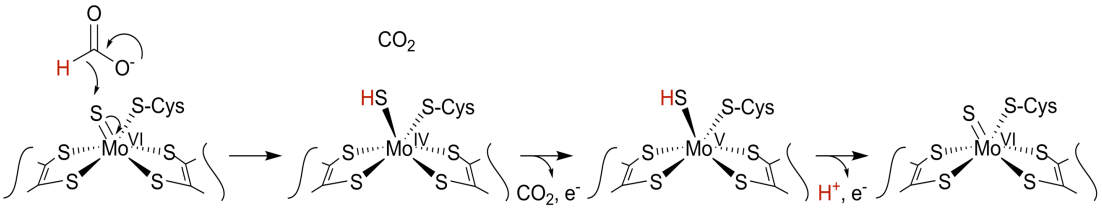

Figure 2.1 *The proposed hydride transfer mechanism for the formate dehydrogenases: as the second carbon-oxygen double bond of the substrate forms, the displaced hydride attacks the Mo=S moiety, resulting in the formal two-electron reduction of the metal.*

Formate is in fact known to be an effective hydride donor (as reflected in the reactivity of the metal-independent formate dehydrogenases that catalyze the direct reduction of NAD^+ by formate via a ternary complex mechanism (involving an E•formate•NAD^+ intermediate), and the Mo^{VI}=S group of the molybdenum center is also known to be an

effective hydride acceptor (as in the reaction mechanism of the molybdenum-containing xanthine oxidase[8]). Were the *C. necator* enzyme to be shown to effectively catalyze the reverse reaction, the implication would be that the Mo^{IV}-SH center is an effective hydride donor to CO_2, with the enzyme competent to activate CO_2 for reduction.

We report here that, contrary to an earlier report[6], the FdsABG formate dehydrogenase from *C. necator* is indeed able to effectively catalyze the reduction of CO_2 using NADH as reductant, stoichiometrically generating formate (as confirmed by NMR) with a k_{cat} of 10 s^{-1}. Importantly, we demonstrate that the enzyme's steady-state kinetic parameters in the forward and reverse reactions are consistent with the overall thermodynamics of the reaction. Finally, we establish the reaction conditions necessary to quantify the reverse reaction.

2.3 Materials and methods

2.3.1 Chemicals

All chemicals were purchased from Fisher Scientific, except where otherwise specified. NAD^+, NADH and ^{13}C-CO_2 were purchased from Sigma-Aldrich (St. Louis, MO), Argon and CO_2 from Airgas, and sodium ^{13}C-bicarbonate from Cambridge Isotope Labs.

2.3.2 Protein Preparation.

Cupriavidus necator (formerly known as *Ralstonia eutropha*) strain HF210 was grown as previously described[11]. All protein purification steps were performed at 0-4°C

with an AKTA FPLC system (GE Healthcare) in a procedure modified from that of Niks *et al.*, 2016[11]. The butyl-4 Sepharose column was replaced with a 1.6 x 22 cm butyl Sepharose HP (GE Healthcare), while the 5 ml butyl Sepharose HP step at the end of the procedure was omitted.

Routine activity assays were performed at 30˚C in 75 mM K-PO_4, pH 7.7 with 2 mM NAD^+ and 40 mM sodium formate; formation of NADH was monitored at 340 nm (ε= 6,220 M^{-1} cm^{-1}), with one unit of activity being defined as the amount of enzyme catalyzing the reduction of 1 μmol of NAD^+ per min. Typically 10 secs were used to calculate the initial slope. Enzyme concentrations were determined using an estimated extinction coefficient at 410 nm of 51,500 M^{-1} cm^{-1} and activities were calculated with respect to one trimer with a molecular weight of 178 kDa[11].

2.3.3 Kinetic Characterization.

Kinetic assays were performed under anaerobic conditions at 30˚C. Dissolved carbon dioxide gas in reaction buffer was used as the source of CO_2. For measuring the effect of pH on k_{obs}, an overlapping buffer system consisting of 75 mM malate, 75 mM potassium phosphate, and 75 mM Tris base were used to cover the pH 4-9 range. All the reaction buffers were first bubbled with carbon dioxide continuously and titrated with potassium hydroxide or hydrochloric acid until the target pH stabilized. Upon addition of 200 μM NADH to each buffer, the solution was filtered and stored in a septum-sealed vial (Wheaton). Immediately before use each vial was resaturated with CO_2 and the solution was transferred to an argon-purged, quartz cuvette sealed with a rubber stopper using an

argon-purged gastight syringe (Hamilton). Reactions were started with addition of enzyme, injected via an argon-purged gastight syringe. The CO_2-reduction activities were measured by the change in NADH absorbance at 340 nm. The first 10 sec after addition of the enzyme were used to calculate the initial slope. Values for k_{obs} were fitted to the equation for a double-ionization mechanism as previously described[11].

To measure the effect of ion strength on k_{obs} and the steady-state parameters for the reaction of FdsABG with NADH, the same experimental setup was used as above, other than that 100 mM K-PO_4, pH 7.0 buffer was using instead of the overlapping buffer system. A range of 9-300 μM NADH was used in these assays and the results were plotted according to the Michaelis-Menten equation for calculating the K_m and k_{cat} values using SigmaPlot.

To measure the steady-state parameters for the reaction of FdsABG with CO_2, 100 mM K-PO_4, pH 7.0 buffer was using for maintaining the pH. Three septa-sealed vials were used in these experiments. Vial A contained the buffer with 200 μM NADH and saturated with CO_2, vial B contained the buffer with 200 μM NADH and saturated with argon, and vial C was flushed with argon and used for mixing reaction buffers from vial A and vial B for generating different concentrations of dissolved CO_2. A range of 0.8-29.5 mM aqueous CO_2 was used in these assays and the results were plotted according to the Michaelis-Menten equation for calculating the K_m and k_{cat} values.

To demonstrate the ability of FdsABG to catalyze both the forward and reverse directions, a reaction was performed in a septum-sealed quartz cuvette which contained the

200 μM NADH in 100 mM K-PO_4, final pH ~ 6.3, saturated with CO_2. FdsABG and formate were injected into the cuvette during the reaction via an argon-purged gastight syringe.

2.3.4 Formic Acid Detection and Identification.

A solution containing 20 mM Bis-Tris propane buffer and 200 μM NADH was first saturated with CO_2 in a septum-sealed quartz cuvette (final pH ~ 6.3). The reaction was started with injection of FdsABG with an argon-purged gastight syringe; the reaction was allowed to proceed until NADH was no longer consumed. The amount of formic acid produced was estimated spectrophotometrically by the change in NADH absorbance at 340 nm. The formate-containing solution was subsequently separated from the enzyme via ultrafiltration with Amicon Ultra 4 (Millipore). The eluate was finally analyzed by ion chromatography (Dionex DX-120), using a Dionex Ionpac AS22 4 X 250 mm column and 4.5 mM sodium carbonate/1.4 mM sodium bicarbonate as eluent with flow rate of 0.49 mL/min. A range of 0-200 μM formic acid dissolved in 20 mM Bis-Tris propane buffer was used for standard calibration; the detection limit was estimated at 10 μM formic acid. At completion of the reaction, the formate was detected with a characteristic retention of 5.9 minutes.

NMR spectroscopy was performed using a Bruker Avance III 700 instrument fitted with a 5 mm TCI ^{1}H, ^{2}H, ^{13}C, ^{15}N quadruple resonance, z-gradient, cryoprobe, optimized for ^{1}H and ^{13}C. A solution containing 20 mM Bis-Tris propane buffer, 6 mM NADH and 10 % D_2O (for NMR frequency lock) was first saturated with $^{13}CO_2$ in a septum-sealed

quartz cuvette with a 4 mm path length (final pH ~ 6.3). The reaction was started by injection of FdsABG using an argon-purged gastight syringe; the reaction was allowed to proceed until NADH was no longer consumed (monitored at 388 nm). The formate-containing solution was subsequently separated from the enzyme via ultrafiltration using an Amicon Ultra 4 (Millipore) filter and the eluate submitted for NMR analysis. A separate NMR standard sample was prepared by bringing a solution of 20 mM Bis-Tris propane and 100 mM natural abundance formic acid to pH ~ 6.3 with a mixture of ^{13}C-labeled and natural abundance sodium bicarbonate (10 % D_2O was added prior to NMR analysis). The bicarbonate resonance was set to 161.08 ppm (calibrated relative to methanol[12]).

2.4 Results

2.4.1 Demonstration of CO_2 as substrate for the reverse reaction.

Carbon dioxide dissolved in aqueous solution exists in many forms: CO_2(aq), carbonic acid, carbonate, and bicarbonate[13]. In a hydride transfer mechanism for the oxidation of formate by FdsABG, the product of the reaction is CO_2 rather than bicarbonate, with the implication that CO_2 rather than bicarbonate is the substrate in the reverse direction. To ascertain whether this is in fact the case, we performed steady-state experiments whose results are summarized in Figure 2.2.

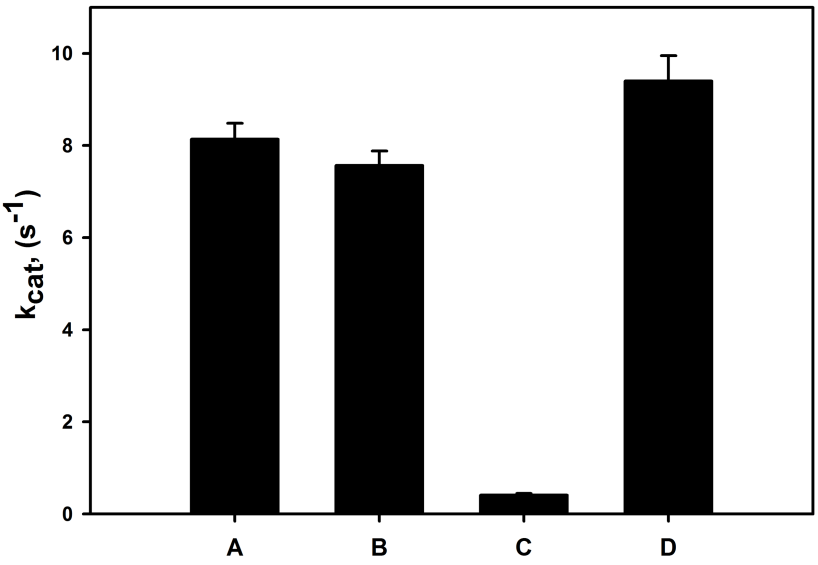

Figure 2.2 *Reaction of FdsABG: under aerobic conditions in the presence (A) or in the absence (B) of 100 mM potassium bicarbonate. Reaction of FdsABG under anaerobic conditions in the presence of bicarbonate (C) or in the presence of saturated CO_2(aq) (D). All reactions were measured by the change in NADH absorbance at 340 nm and performed in 100 mM K-PO_4 at pH 7.0 and 30˚C.*

First, we measured the ability of FdsABG to catalyze the reverse reaction using 100 mM potassium bicarbonate as the substrate at pH 7.0 and 30˚C under aerobic conditions, monitoring the reaction by the oxidation of NADH; the resulting rate was determined to be 8.1 s^{-1}. Significantly, a control experiment performed in the absence of bicarbonate yielded a similar rate, indicating that the observed oxidation of NADH by FdsABG was due to the diaphorase (O_2 : NADH oxidoreductase) activity of the enzyme. Additionally, in the presence of bicarbonate, but in the absence of O_2, NADH oxidation was virtually eliminated. Finally, we performed an anaerobic experiment with a saturated solution of

CO_2 as the substrate; the resulting rate was determined to be 9.4 s^{-1}. Under our experimental conditions (30˚C, 1 atm, pH 7.0) the amount of CO_2(aq) in solution under saturating conditions was calculated as 29.5 mM, with potassium bicarbonate concentration of approximately 139 mM (at this pH there are only trace amounts of carbonic acid or carbonate)[13]. The implication of the above experiments is thus that the substrate for the reverse reaction is CO_2(aq), rather than carbonic acid, carbonate, or bicarbonate.

2.4.2 pH dependence of the reverse reaction.

We next examined the pH dependence of the kinetics of the reverse reaction, with all experiments performed under anaerobic conditions. In these experiments, we performed duplicate assays at each pH using CO_2–saturated solutions and solutions that were 50% CO_2 to confirm that we were working at the high concentration limit of CO_2 (control data not shown). As illustrated in Figure 2.3 (data in black), the reaction of FdsABG with CO_2 has a nominal pH optimum around 7.0. The values for k_{obs} were fitted to the equation for a double-ionization mechanism, which yielded two apparent pK_a values of 5.5 and 8.3. Both pK_a values are in reasonable agreement with those measured for the reaction of FdsABG with formate (5.6 and 9.3, respectively). We note, however, that the value for pK_{a2}^{eff} may be subject to considerable error as a result of the increasing ionic strength of the CO_2-saturated solutions at higher pH. Because the total dissolved carbon increases exponentially with pH as a result of increased concentrations of bicarbonate (and eventually carbonate), the ionic strength of CO_2-saturated solutions also increases very significantly, as reflected by the increased conductivity at high pH (Figure 2.3, data in blue); the conductivity reflects

not only the amount of total carbon species but significant concentrations of K^+ as a consequence of adjusting pH with KOH. Contributions to total carbon from bicarbonate and carbonate can be calculated from well-defined temperature-related equilibrium constants and partial pressures according to Equations 2.2 and 2.3, below:

$$\log[HCO_3^-] = \log K_H + \log K_{a1} + \log P_{CO_2} + pH \quad \text{(Eq. 2.2)}$$

$$\log[CO_3^{2-}] = \log K_H + \log K_{a1} + \log K_{a2} + \log P_{CO_2} + 2pH \quad \text{(Eq. 2.3)}$$

where K_H, K_{a1}, K_{a2} are the acid dissociation constants for CO_2(aq), HCO_3^-, CO_3^{2-}, respectively, and P_{CO_2} is the partial pressure of CO_2 [13]. We tested the effect of increasing ionic strength on the ability of the enzyme to catalyze both the forward and reverse reactions. The $k_{cat}^{CO_2}$ for the reaction of FdsABG with CO_2 decreased to 13% in the presence of 3M KCl (Figure 2.4). The reaction of FdsABG with formate was similarly affected by increasing ionic strength; $k_{cat}^{formate}$ decreased to 13% in the presence of 4M KCl (Figure 2.4). It is thus likely that the decrease in activity above pH 7.0 as described by pK_{a2}^{eff} was principally due to ionic strength effects rather than ionization phenomena. The identity of the ionizable group whose protonation results in loss of activity at low pH is not known, although a likely candidate is the Mo^{VI}=S group of the molybdenum center, which is known to be protonated at pH 7.0 upon reduction of the molybdenum[11].

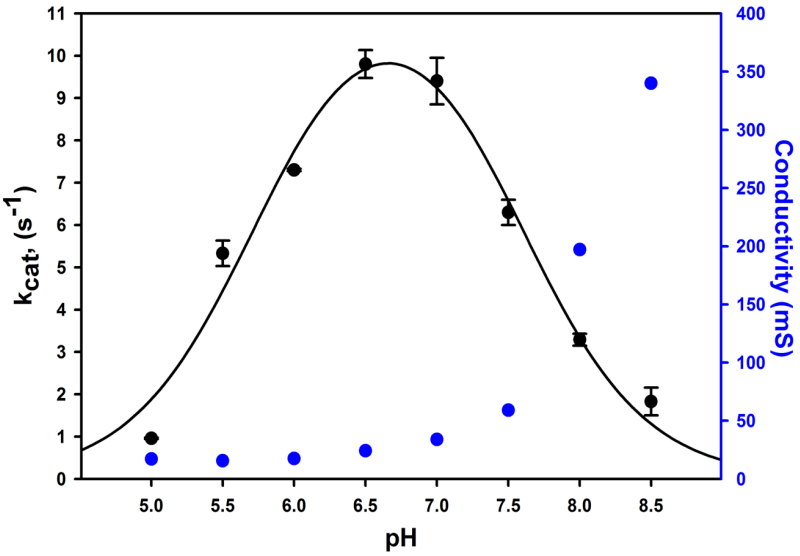

Figure 2.3 *The dependence of k_{cat} for FdsABG on pH. Kinetic experiments were performed using an overlapping buffer system (75 mM each of malate, potassium phosphate, and Tris base), containing 200 µM NADH and saturated with CO_2(aq). The fit to the data (black solid line) yielded two pKa values of pKa^1 = 5.5 and $pKa2^{eff}$ = 8.3. A plot in blue represents the corresponding conductivity, a consequence of increasing concentrations of bicarbonate/carbonate as well as KOH. All reactions were performed at 30˚C under anaerobic conditions.*

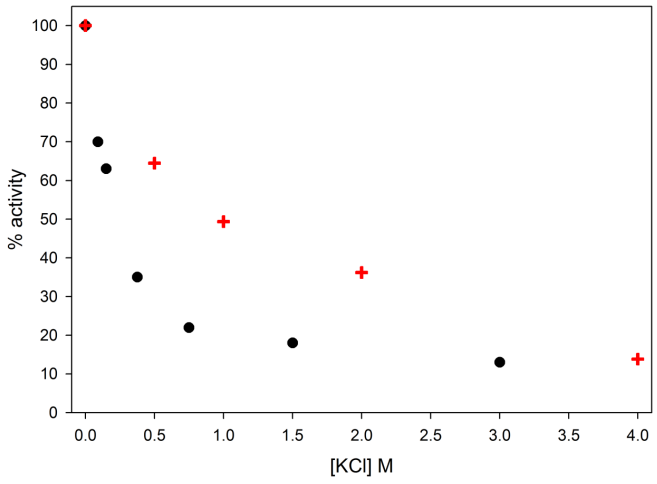

Figure 2.4 *Effect of KCl concentration on the reaction of FdsABG with saturated CO_2 and 200 µM NADH (black circles) or 40 mM formate and 2 mM NAD^+ (red crosses). All reactions were performed in 100 mM K-PO_4 at pH 7.0 at 30˚C.*

2.4.3 Further analysis of the reverse reaction.

To demonstrate the ability of FdsABG to catalyze the reaction in both the forward and reverse directions, an experiment was performed in which the enzyme was sequentially supplemented with NAD^+ or formate in a septum-sealed quartz cuvette under anaerobic conditions. Upon addition of enzyme to a cuvette containing 200 μM NADH in 100 mM potassium phosphate saturated with CO_2 (final pH 6.3; arrow 1, Figure 2.5), an absorbance decrease was observed as NADH was partially consumed upon catalysis of the reverse reaction, the reaction being driven by the high concentration of CO_2 in the reaction mix. The reaction was allowed to proceed until NADH was no longer consumed, at which point the cuvette contained formate produced from CO_2 reduction and an equivalent amount of NAD^+. 400 μM NAD^+ was injected to drive the reaction in the reverse direction (Figure 2.5, arrow 2), with an absorbance increase as NAD^+ was reduced back to NADH. The reaction was allowed to proceed until NADH was no longer produced, at which point the solution was supplemented with 40 mM formate (Figure 2.5, arrow 3), which resulted in a further absorbance increase as more NAD^+ was reduced to NADH at the expense of the initially formed formate. These results confirm the thermodynamic and kinetic competence of the enzyme to catalyze both the forward and reverse reactions.

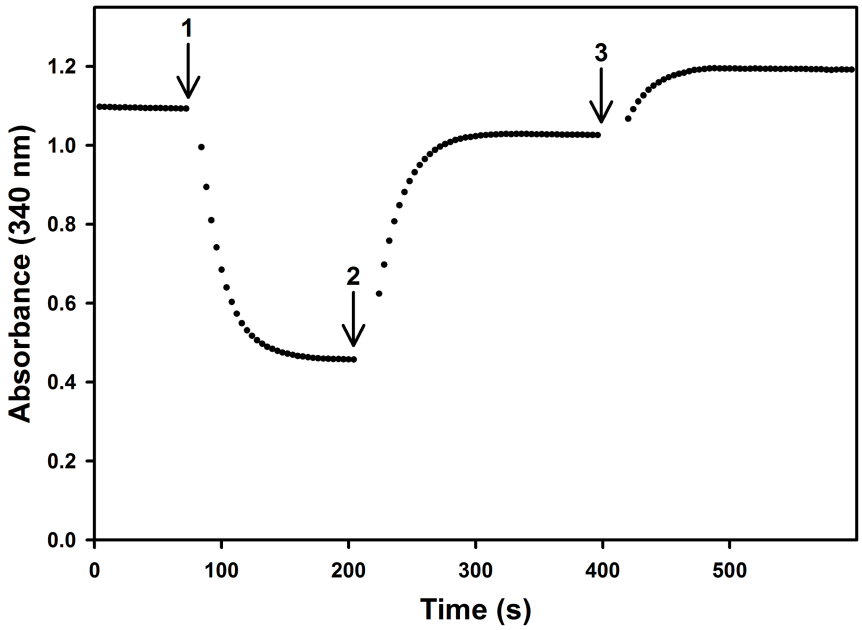

Figure 2.5 *Demonstration of the ability of FdsABG to catalyze both CO_2 reduction and formate oxidation. The reaction was initiated by addition of FdsABG (arrow 1) via an argon-purged gastight syringe to 200 µM NADH in 100 mM phosphate, saturated with CO_2(aq); final pH 6.3. At approximately 200 s, 400 µM NAD^+ was injected into the cuvette (arrow 2) and the reaction was allowed to proceed. At approximately 400 s, 40 mM formate was further injected into the cuvette (arrow 3). The reaction was performed at 30˚C under anaerobic conditions.*

2.4.4 Formic Acid Quantificaton and Identification.

Next, we confirmed by ion chromatography that the reaction product of the reduction of CO_2 catalyzed by FdsABG was in fact formic acid, using the protocol described in the experimental procedures section. FdsABG was incubated with anaerobic, saturated CO_2(aq) and 300 µM NADH in 20 mM Bis-Tris propane (final pH 6.3, 30˚C) and the reaction followed by the absorbance decrease at 340 nm (Figure 2.7A). At completion of the reaction, an aliquot was withdrawn and submitted to ion chromatography, with formate being detected with a characteristic retention of 5.9 minutes

(Figure 2.7B). Comparison against a calibration curve (Figure 2.6) yielded a value of 120 μM of formic acid generated in the experiment, which was in very good agreement with the 130 μM NADH consumed on the basis of the absorbance change at 340 nm. These results demonstrate the stoichiometric generation of formic acid at the expense of NADH for the enzyme-catalyzed reaction in the reverse direction. The identity of formic acid/formate generated enzymatically was further confirmed by comparison of the ^{13}C-NMR spectrum with an authentic natural abundance formic acid standard (Figure 2.7C-D).

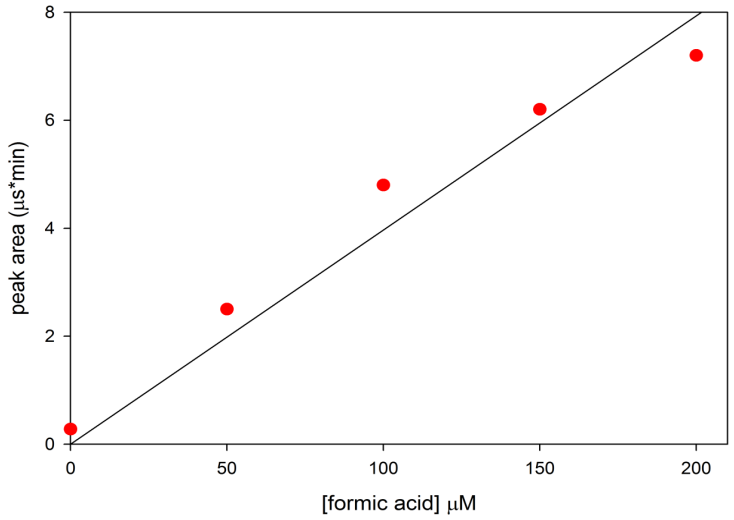

Figure 2.6 *Calibration standard curve (with slope = 0.038) for formic acid using Ion Chromatography.*

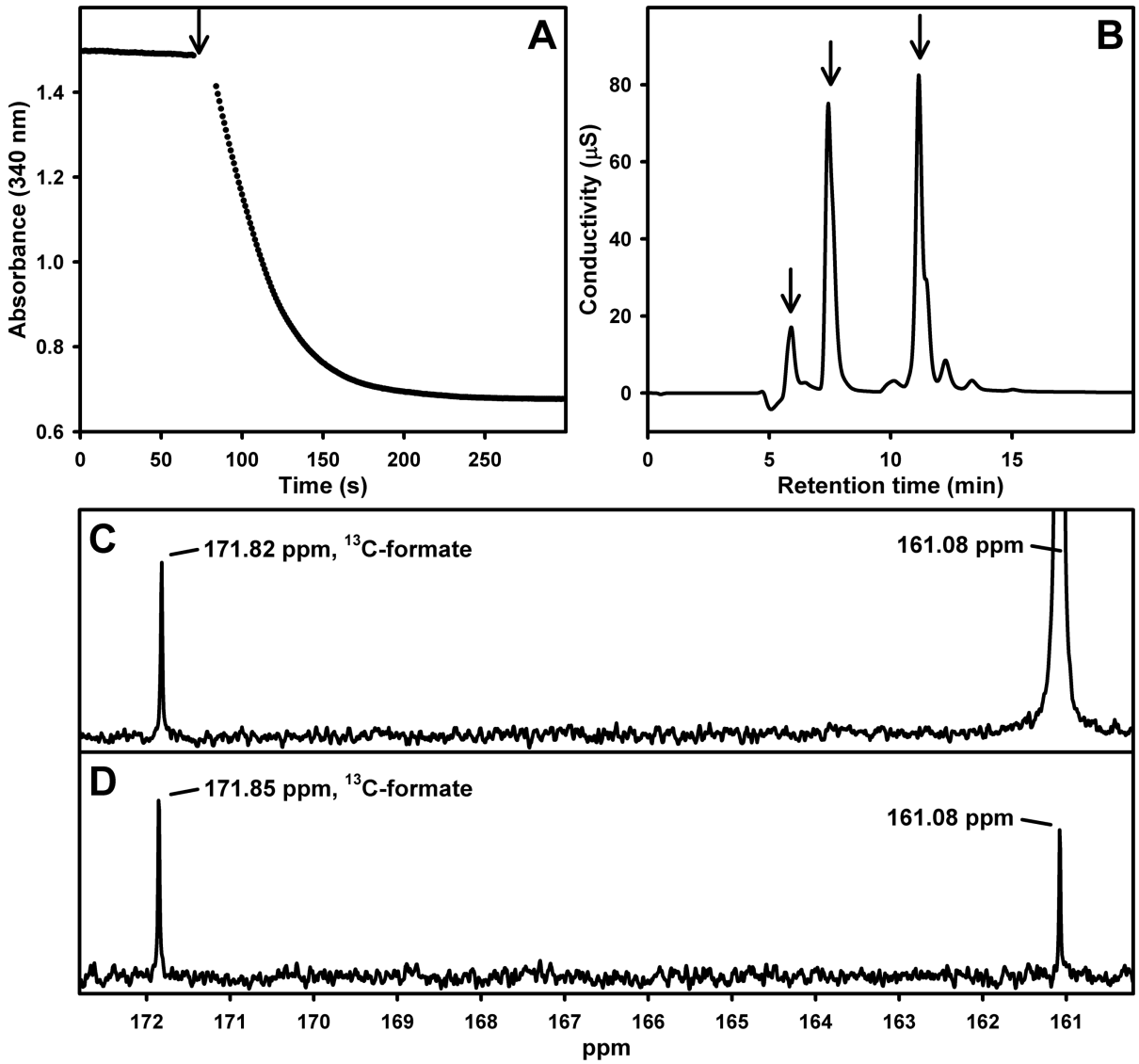

Figure 2.7 (A) *Reaction of FdsABG with saturated CO_2(aq) and 300 μM NADH in 20 mM Bis-Tris propane (final pH 6.3), performed at 30˚C under anaerobic conditions. Arrow indicates addition of enzyme.* ***(B)*** *Ion chromatography analysis of the product of the reaction in (A) as described in the experimental procedures section. Retention times are indicated with arrows for formate (5.9 min), bicarbonate (7.4 min) and NADH/NAD^+ (11.2 min).* ***(C)*** *^{13}C-NMR spectrum for ^{13}C-formate generated enzymatically with dissolved ^{13}C-bicarbonate at 161.08 ppm.* ***(D)*** *^{13}C-NMR standard spectrum with 100 mM natural abundance formic acid brought to pH ~ 6.3 with sodium bicarbonate.*

2.4.5 Enzyme kinetics.

Finally, with the reversibility of the reaction fully established, we sought to determine k_{cat}, $K_m^{CO_2}$ and K_m^{NADH} for the reverse reaction. Having previously demonstrated that FdsABG operates via a ping-pong mechanism[11], the experiments simply involved determining the dependence of k_{obs} as a function of [CO_2] at a saturating concentration of NADH, and as a function of [NADH] at a kinetically saturating concentration of CO_2. As shown in Figure 2.8, the results yielded hyperbolic plots from which a k_{cat} of 10 s^{-1}, a $K_m^{CO_2}$ of 2.7 mM (Figure 2.8A) and a K_m^{NADH} of 46 μM at pH 7.0 (Figure 2.8B) could be obtained. The k_{cat} for CO_2 reduction is some 14 times slower than k_{cat} for formate oxidation by FdsABG.

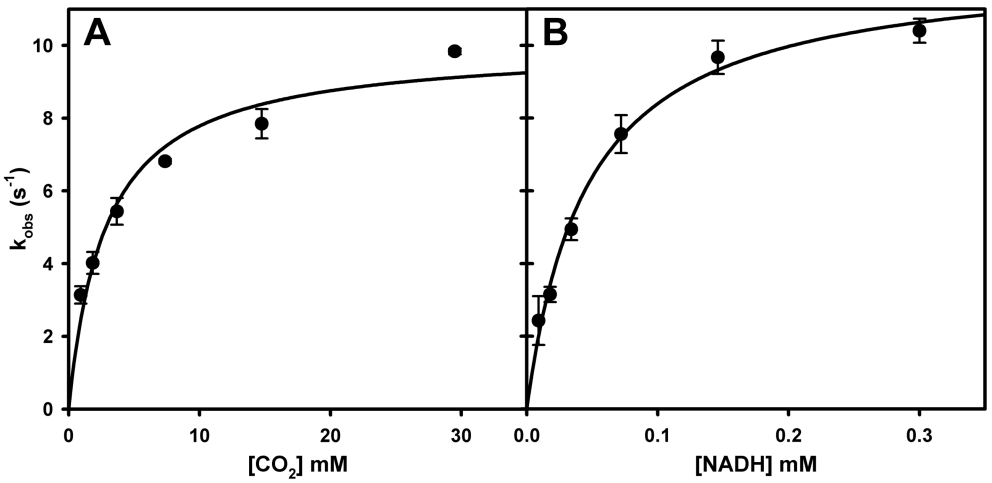

Figure 2.8 *(A) Hyperbolic plots for the reaction of FdsABG with CO_2(aq) in the presence of 200 μM NADH. (B) Hyperbolic plots for the reaction of FdsABG with NADH in the presence of saturated CO_2(aq). Plots in (A) and (B) yielded a k_{cat} of 10 s^{-1}, a Km^{CO_2} of 2.7 mM and a Km^{NADH} of 46 μM, respectively. All reactions were performed in 100 mM K-PO_4, pH 7.0 at 30˚C under anaerobic conditions.*

2.5 Discussion

The FdsABG formate dehydrogenase from *C. necator* has been reported previously to be unable to catalyze the reverse reaction of formate oxidation[6, 7, 9]. The method used in this earlier work was similar to that employed here, and we are unable to account for their (false) negative result. It was stated that a long (40-minute) incubation period was used, however, and it is possible that the enzyme lost substantial activity over this period of time. In the present work we find that the enzyme is in fact quite effective catalyzing the reduction of CO_2, being able to stoichiometrically transfer reducing equivalents from NADH to CO_2 with a steady-state k_{cat} of 10 s^{-1}. Given the previously observed false negative results with this (and possibly other) formate dehydrogenases, two specific points are important to bear in mind assessing the ability of a given enzyme to catalyze the reverse reaction: first, the product of the reaction in the forward direction (and hence the substrate in the reverse) is CO_2 rather than bicarbonate; and second, the reverse assay must be carried out under anaerobic conditions to avoid consumption of NADH by possible diaphorase activity of the enzyme. It must also be kept in mind that the pH optimum for the reverse reaction may be perturbed by ion strength effects given the higher concentration of bicarbonate/carbonate at higher pH.

Bicarbonate/carbonate is routinely used as a source for CO_2 in aqueous solutions, but it is important to recognize that it is an imperfect one. Although some equilibrium concentration of CO_2 will always eventually be obtained, the uncatalyzed interconversion of CO_2 and bicarbonate in aqueous solutions is in fact very sluggish on the timescales of

catalysis for all formate dehydrogenases, even at low pH where CO_2 is expected to predominate at equilibrium. Further, for reactions performed in experimental apparatus having a significant volume of headspace, partitioning into the gas phase will lower the concentration of dissolved CO_2 for any given amount of bicarbonate/carbonate added. The final concentration of dissolved CO_2 will in fact ultimately be dictated by the partial pressure of CO_2 in the headspace according to Henry's Law, not simply the total amount of bicarbonate initially added. It is likely that these considerations have all contributed to false negative results in assessing whether one or another formate dehydrogenase is capable of catalyzing the reduction of CO_2 to formate. Our observation that, at least with the FdsABG formate dehydrogenase, there is significant diaphorase (O_2 : NADH oxidoreductase) activity that consumes NADH regardless of whether formate is formed by hydride transfer to CO_2, further underscores the importance of performing assays under anaerobic conditions. It is a key aspect of the present work that we have not simply identified a(nother) formate dehydrogenase capable of reducing CO_2 under the appropriate conditions but provided and explanation for the disparate and confusing results of previous studies with this and other enzymes.

From a thermodynamic stand point, E_0' for the NADH/NAD^+ couple is -320 mV and that for the formate/CO_2 couple is -420 mV. From the Nernst equation, the overall K_{eq} for the two-electron process is calculated to be approximately 2100. To ensure compliance with the First Law of Thermodynamics, the following Haldane relationship (Equation 2.4)

relating the steady-state parameters for an enzyme operating via a ping-pong mechanism holds[14]:

$$K_{eq} = \frac{\dfrac{k_{cat}^{forward}}{K_m^{formate}} \cdot \dfrac{k_{cat}^{forward}}{K_m^{NAD+}}}{\dfrac{k_{cat}^{reverse}}{K_m^{CO2}} \cdot \dfrac{k_{cat}^{reverse}}{K_m^{NADH}}} \qquad \text{(Eq. 2.4)}$$

$$= \frac{\dfrac{(201\ s^{-1})}{(130\ \mu M)} \cdot \dfrac{(201\ s^{-1})}{(310\ \mu M)}}{\dfrac{(10\ s^{-1})}{(2.7\ mM)} \cdot \dfrac{(10\ s^{-1})}{(46\ \mu M)}}$$

$$= 1250$$

With $k_{cat}^{forward} = 201\ s^{-1}$, $K_m^{formate} = 130\ \mu M$, $K_m^{NAD^+} = 310\ \mu M$ from our previous work[11], and $k_{cat}^{reverse} = 10\ s^{-1}$, $K_m^{CO_2} = 2.7\ mM$, $K_m^{NADH} = 46\ \mu M$ from the present work, the overall calculated K_{eq} from the steady-state parameters is calculated to be 1250, Given the squared dependence of the calculation on $k_{cat}^{forward}$ and $k_{cat}^{reverse}$, the agreement with the value of 2100 determined from the Nernst equation is considered to be quite good. This constitutes a stringent test of the validity of the steady-state parameters in both the forward and reverse reactions.

Moura and coworkers have recently examined the reaction of the periplasmic formate dehydrogenase from *Desulfovibrio desulfuricans* and have concluded that this

reaction also proceeds via a hydride transfer mechanism[15]. Like the *C. necator* enzyme studied here, the *D. desulfuricans* enzyme possesses a terminal Mo^{VI}=S sulfide group in the oxidized state but has a selenocysteine ligand to the molybdenum in place of the cysteine residue seen in FdsABG. The *D. desulfuricans* enzyme also differs in passing reducing equivalents into the intramembrane quinone pool (via subunits possessing four *c*-type cytochromes and two [4Fe-4S] clusters) rather than reducing NAD^+, and thus these workers necessarily used reduced methyl viologen as a non-physiological reductant. It was not possible to assess the overall thermodynamics of the reverse reaction and the validity of the Haldane relationship as done here.

The active sites in the metal-dependent (both molybdenum- and tungsten-containing) formate dehydrogases all possess a common active site structure, as shown in Figure 2.9. The present results strongly suggest that all operate via the same hydride transfer mechanism, and likely they all do so fully reversibly under the appropriate experimental conditions. The majority of these enzymes function physiologically in the direction of formate oxidation, but the molybdenum-dependent formate:hydrogen lyase complex of the acetogen *Acetobacterium woodii* has recently been shown to function physiologically in the direction of CO_2 reduction, using reducing equivalents obtained from H_2 [16, 17]. The hydride transfer mechanism is also likely to be relevant to both the molybdenum- and tungsten-containing formyl-methanofuran dehydrogenases from methanogenic bacteria. These enzymes catalyze the first step in methanogenesis, the reductive condensation of CO_2 and methanofuran to yield formylmethanofuran; they are

bifunctional, with a molybdenum or tungsten center involved in the oxidation-reduction reaction in one subunit and a di-zinc center that binds the methanofuran substrate in a second. The molybdenum- and tungsten-containing active sites of this second group of enzymes also strongly resemble those seen in the above-mentioned formate dehydrogenases seen in Figure 2.9.

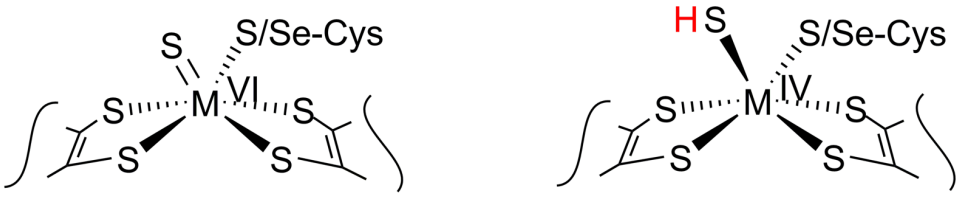

Figure 2.9 *Active site structures for formate dehydrogenases and formylmethanofuran dehydrogenases: oxidized and reduced forms, respectively.*

The tungsten-containing enzyme from *Thermomethanobacter wolfeii* has recently been characterized crystallographically, with the surprising observation that the tungsten and di-zinc active sites are separated by some 43 Å, with an intraprotein tunnel connecting them[18]. The reaction had been thought to proceed via condensation of CO_2 with methanofuran to form carboxymethanofuran, followed by reduction of this intermediate to product formylmethanofuran. Given the structure of the enzyme, however, with the methanofuran binding site so far removed from the tungsten center where reduction occurs, it is clear that the reaction must instead proceed via reduction of CO_2 to formate at the tungsten center, followed by diffusion of the formate thus formed through the intraprotein tunnel to the di-zinc site, where it condenses with methanofuran to give the formylmethanofuran. The reaction at the tungsten sites of these enzymes is exactly

equivalent to the reverse of the FdsABG formate dehydrogenase considered here, and it also likely proceeds via a hydride transfer mechanism (it being known that CO_2 rather than bicarbonate is the substrate for the enzyme). Again, all these systems in their oxidized states have active sites with the structure shown in Figure 2.9, where the oxidized active site can be formulated as $L_2M^{VI}S$(S/Se-Cys), with M being either Mo or W; the reduced active site is formulated as L_2M^{IV}(SH)(S/Se-Cys). We suggest that all these systems function via the same basic hydride transfer mechanism regardless of the physiological direction of the reaction, with the oxidized M^{VI}=S moiety constituting an effective hydride acceptor from formate and the reduced M^{IV}-SH moiety an effective hydride donor to CO_2. The mechanistic corollary is that just as formate is an effective hydride donor in the one direction, CO_2 is an effective hydride acceptor in the reverse. With regard to the specific manner in which these enzymes activate CO_2 for reduction, it is noteworthy that the active sites of these enzymes possess two strictly conserved Arg and His residues (illustrated in Figure 2.10 in the case of the FdhF formate dehydrogenase from *E. coli* [19]) that are known to be involved in formate binding in the forward direction and which we suggest are well-positioned to accommodate the accumulating negative charge and molecular dipole on CO_2 as the transition state in the reverse direction forms.

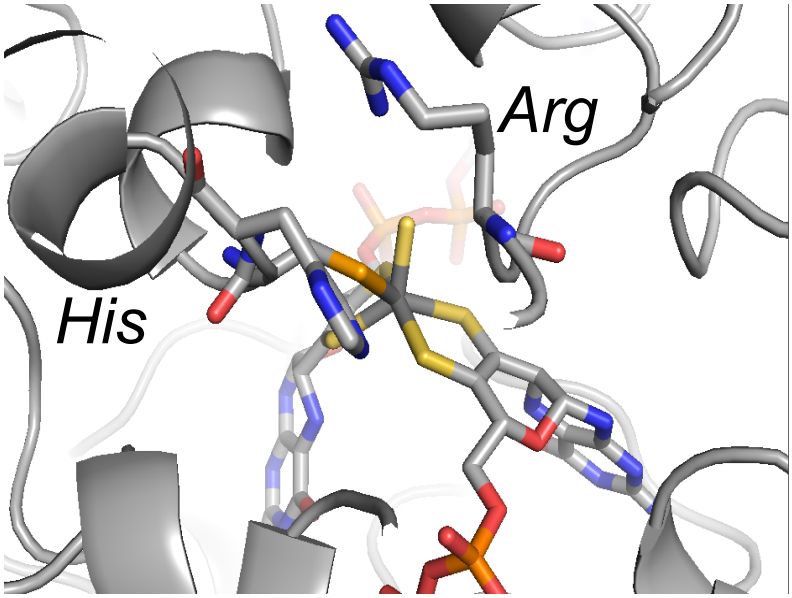

Figure 2.10 *The active site of the FdhF formate dehydrogenase from E. coli. The highly conserved Arg and His residues implicated in formate binding are indicated.*

The ability to reduce CO_2 rapidly and efficiently has taken on great importance over the past decade, linked as it is to the emergence of inexpensive and sustainable sources of electricity[20]. A variety of biohybrid systems have been developed utilizing metal-dependent formate dehydrogenases from a variety of organisms to bring about electrochemically driven reduction of CO_2 to formate (reviewed in refs. [16, 21, 22]). In this context the importance of the present work is twofold: first, the conditions are now identified under which the ability of a given enzyme to catalyze the reduction of CO_2 can be assessed; and second, that the reaction mechanism utilized by all these enzymes involves hydride rather than H_2 as reductant, with formate rather than formic acid being generated. Even in the case of the *A. woodii* system ([16, 17]), H_2 is oxidized to electrons and protons at the di-iron site of the hydrogenase component, with the electrons subsequently transferred

to the molybdenum center of the formate dehydrogenase component, which reduces CO_2 via hydride transfer. The now-demonstrated ability of biological systems to utilize a lower-barrier reaction for CO_2 reduction involving the reaction of hydride to yield formate, rather than H_2 to yield formic acid, has significant implications for the development of improved biohybrid and synthetic systems for CO_2 fixation.

2.6 Conclusions

We have characterized here the kinetics of the reverse reaction for the molybdenum-containing FdsABG formate dehydrogenase of *C. necator* using CO_2 as the reaction substrate and shown that the relevant Haldane relationship holds for the steady-state kinetic parameters in the forward and reverse reaction. We have further quantified for the first time the stoichiometric accumulation of formic acid as the product of the reaction and demonstrated the importance of performing enzymatic experiments with CO_2 under anaerobic conditions, as detailed in the experimental procedures section. We submit that all molybdneum- and tungsten-containing enzymes of the formate dehydrogenase family, including the formymethanofuran dehydrogenases, operate via the same hydride transfer mechanism, and do so fully reversibly. The present work thus provides a framework for the development of increasingly efficient biocatalytic processes for CO_2 fixation.

2.7 References

1. Maia, L. B.; Moura, J. J. G.; Moura, I., Molybdenum and tungsten-dependent formate dehydrogenases. Journal of Biological Inorganic Chemistry 2015, 20 (2), 287-309.

2. Sun, Q.; Jiang, Y.; Jiang, Z.; Zhang, L.; Sun, X.; Li, J., Green and Efficient Conversion of CO_2 to Methanol by Biomimetic Coimmobilization of Three Dehydrogenases in Protamine-Templated Titania. Industrial & Engineering Chemistry Research 2009, 48 (9), 4210-4215.

3. Olah, G. A., Beyond oil and gas: The methanol economy. Angewandte Chemie-International Edition 2005, 44 (18), 2636-2639.

4. Qiao, J.; Liu, Y.; Hong, F.; Zhang, J., A review of catalysts for the electroreduction of carbon dioxide to produce low-carbon fuels. Chemical Society Reviews 2014, 43 (2), 631-675.

5. Maia, L. B.; Moura, I.; Moura, J. J. G., Molybdenum and tungsten-containing formate dehydrogenases: Aiming to inspire a catalyst for carbon dioxide utilization. Inorganica Chimica Acta 2017, 455, 350-363.

6. Friedebold, J.; Bowien, B., Physiological and biochemical characterization of the soluble formate dehydrogenase, a molybdoenzyme from *Alcaligenes eutrophus*. Journal of Bacteriology 1993, 175 (15), 4719-4728.

7. Pohlmann, A.; Fricke, W. F.; Reinecke, F.; Kusian, B.; Liesegang, H.; Cramm, R.; Eitinger, T.; Ewering, C.; Potter, M.; Schwartz, E.; Strittmatter, A.; Voss, I.; Gottschalk, G.; Steinbuchel, A.; Friedrich, B.; Bowien, B., Genome sequence of the bioplastic-producing "Knallgas" bacterium Ralstonia eutropha H16. Nature Biotechnology 2006, 24 (10), 1257-1262.

8. Hille, R.; Hall, J.; Basu, P., The Mononuclear Molybdenum Enzymes. Chemical Reviews 2014, 114 (7), 3963-4038.

9. Oh, J. I.; Bowien, B., Structural analysis of the fds operon encoding the NAD($^+$)-linked formate dehydrogenase of *Ralstonia eutropha*. Journal of Biological Chemistry 1998, 273 (41), 26349-26360.

10. Sazanov, L. A.; Hinchliffe, P., Structure of the hydrophilic domain of respiratory complex I from *Thermus thermophilus*. Science 2006, 311 (5766), 1430-1436.

11. Niks, D.; Duvvuru, J.; Escalona, M.; Hille, R., Spectroscopic and Kinetic Properties of the Molybdenum-containing, NAD(+) - dependent Formate Dehydrogenase from *Ralstonia eutropha*. Journal of Biological Chemistry 2016, 291 (3), 1162-1174.

12. Gottlieb, H. E.; Kotlyar, V.; Nudelman, A., NMR chemical shifts of common laboratory solvents as trace impurities. Journal of Organic Chemistry 1997, 62 (21), 7512-7515.

13. Butler, J. N., Carbon Dioxide Equilibria and Their Applications. Taylor & Francis: 1991.

14. Segel, I. H., Enzyme Kinetics: Behavior and Analysis of Rapid Equilibrium and Steady-State Enzyme Systems. Wiley: 1993.

15. Maia, L. B.; Fonseca, L.; Moura, I.; Moura, J. J. G., Reduction of Carbon Dioxide by a Molybdenum-Containing Formate Dehydrogenase: A Kinetic and Mechanistic Study. Journal of the American Chemical Society 2016, 138 (28), 8834-8846.

16. Schuchmann, K.; Mueller, V., Direct and Reversible Hydrogenation of CO_2 to Formate by a Bacterial Carbon Dioxide Reductase. Science 2013, 342 (6164), 1382-1385.

17. Schuchmann, K.; Muller, V., Autotrophy at the thermodynamic limit of life: a model for energy conservation in acetogenic bacteria. Nature Reviews Microbiology 2014, 12 (12), 809-821.

18. Wagner, T.; Ermler, U.; Shima, S., The methanogenic CO_2 reducing-and-fixing enzyme is bifunctional and contains 46 4Fe-4S clusters. Science 2016, 354 (6308), 114-117.

19. Boyington, J. C.; Gladyshev, V. N.; Khangulov, S. V.; Stadtman, T. C.; Sun, P. D., Crystal structure of formate dehydrogenase H: Catalysis involving Mo, molybdopterin, selenocysteine, and an Fe4S4 cluster. Science 1997, 275 (5304), 1305-1308.

20. Appel, A. M.; Bercaw, J. E.; Bocarsly, A. B.; Dobbek, H.; DuBois, D. L.; Dupuis, M.; Ferry, J. G.; Fujita, E.; Hille, R.; Kenis, P. J. A.; Kerfeld, C. A.; Morris, R. H.; Peden, C. H. F.; Portis, A. R.; Ragsdale, S. W.; Rauchfuss, T. B.; Reek, J. N. H.; Seefeldt, L. C.; Thauer, R. K.; Waldrop, G. L., Frontiers, Opportunities, and Challenges in Biochemical and Chemical Catalysis of CO_2 Fixation. Chemical Reviews 2013, 113 (8), 6621-6658.

21. Shi, J. F.; Jiang, Y. J.; Jiang, Z. Y.; Wang, X. Y.; Wang, X. L.; Zhang, S. H.; Han, P. P.; Yang, C., Enzymatic conversion of carbon dioxide. Chemical Society Reviews 2015, 44 (17), 5981-6000.

22. Mondal, B.; Song, J.; Neese, F.; Ye, S., Bio-inspired mechanistic insights into CO_2 reduction. Current Opinion in Chemical Biology 2015, 25, 103-109.

Chapter 3

Synthesis of Formate from CO_2 Gas Catalyzed by an O_2-tolerant NAD-Dependent Formate Dehydrogenase and Glucose Dehydrogenase

3.1 Abstract

Direct conversion of CO_2 to liquid fuel, such as formic acid, through biocatalyst is an attractive option. Formate dehydrogenases (FDHs) are a heterogeneous group of enzymes, which can catalyze the oxidation of formic acid to carbon dioxide with generating two protons and two electrons. Recently, several FDHs have been reported to be able to catalyze the reverse reaction, *i.e.* reduction of carbon dioxide to formic acid under appropriate conditions. The main challenges with these enzymes are that either the CO_2-reducing activity is very low or high oxygen sensitive. Our earlier studies (Yu *et al.* (2017) *J. Biol. Chem.* **292**, 16872-16879) have shown that FdsABG formate dehydrogenase from *Cupriavidus necator* is able to effectively catalyze the reduction of CO_2 with oxygen tolerance. Based on this result, we developed a highly thermodynamic efficient and cost effective biocatalytic process for transformation of the CO_2 to formic acid with using FdsABG. Importantly, we have cloned the full-length soluble formate dehydrogenase (FdsABG) from *C. necator* and expressed in *E. coli* with a His-tag fused to the with the N

terminus of fdsG subunit, and this overexpression system has simplified the FdsABG purification steps from 5-day work to 1-day work compare to protein purification process from native bacteria *C. necator*. We have also combined this engineered *C. necator* FdsABG with another biological enzyme, Glucose Dehydrogenase, for continuous electrons donation to the reaction of converting CO_2 to formate. The results turn out that our engineered *C. necator* FdsABG has a highly thermodynamic efficient to the reduction of CO_2 process with total turnover number of 1.9.

3.2 Introduction

The increasing concentration of carbon dioxide in the atmosphere is a matter of global concern, given the serious environmental and climate implications. An attractive solution is the utilization of the abundantly available "waste" carbon dioxide as a feedstock to produce useful chemicals and liquid fuels[1]. In recent years, formic acid has become a promising liquid fuel, a hydrogen energy carrier with advantages of high volumetric capacity (53 g H_2/L), low toxicity and flammability under ambient conditions, as well as an important feedstock for synthesis of other valuable chemicals[1-4]. A number of heterogeneous catalysts, homogeneous catalysts, electrocatalysts and photocatalysts have been investigated for conversion of carbon dioxide to formic acid[3, 5]. However, low selectivity and yields and requirement of hydrogen, high temperature and high pressure or additional electricity or light energy are major limitations of these methods[3, 6, 7]. In comparison, biocatalysts for the conversion of CO_2 to liquid fuel have the advantages of mild reaction conditions: room temperature under ambient pressure, and neutral pH[5]. Thus,

direct conversion of CO_2 to useful chemicals/liquid fuels, such as formic acid, through biocatalysis is a more attractive option.

Formate dehydrogenases (FDHs) are a heterogeneous group of enzymes, which can catalyze the oxidation of formic acid to carbon dioxide while generating two protons and two electrons[8]. FDHs can be classified into three enzyme categories: metal-independent/$NAD(P)^+$-dependent formate dehydrogenases, metal-containing/$NAD(P)^+$-independent formate dehydrogenases, and metal-containing/$NAD(P)^+$-dependent formate dehydrogenases[8]. Several FDHs have been reported to be able to catalyze the reverse reaction, which is the reduction of carbon dioxide to formic acid under appropriate conditions[9]. FDH from yeast *Candida boidinii* (CbFDH) and FDH from bacteria *Thiobacillus sp.* KNK65MA (TsFDH) are two examples of metal-independent/$NAD(P)^+$-dependent FDHs[10]. CbFDH, in particular, has been widely investigated for reduction of CO_2 in various forms including enzymatic cascade, electrochemical reaction and photochemical reaction[11-14]. However, the problem with these enzymes is that the CO_2-reducing activity is very low (k_{cat} for TsFDH was reported as 0.318 s^{-1} and k_{cat} for CbFDH was reported to be 0.015 s^{-1})[10]. In comparison, the metal-dependent/$NAD(P)^+$-independent FDHs contain tungsten or molybdenum in their active site and have a high CO_2-reducing activity. FDH1 and FDH2 from *Syntrophobacter fumaroxidans* were reported to have an extremely high CO_2-reducing activity with k_{cat} about $2.5x10^3$ s^{-1} and $0.2x10^3$ s^{-1}, respectively[15]. However, these enzymes are extremely oxygen sensitive because of the presence of selenocysteine at the tungsten active site, rendering them unsuitable for

industrial applications. Therefore, an oxygen tolerant and robust enzyme has potential for future industry applications.

The molybdenum-containing/NAD^+-dependent FDH (FdsABG) purified from the bacterium *Cupriavidus necator* (formerly known as *Ralstonia eutropha*) is an O_2-tolerent, soluble homodimer of trimers, $(\partial\beta\gamma)_2$, containing seven iron-sulfur clusters as well as the bis(molybdopterin guanine dinucleotide)molybdenum (bis(MGD)Mo) cofactor and FMN[16-18]. This FdsABG is an unusual enzyme among the metal-dependent formate dehydrogenases family because of the following advantageous properties including: O_2-tolerance, water-solubility and the ability to effectively catalyze the reduction of CO_2 using NADH as a terminal electron donor, stoichiometrically generating formate with a k_{cat} of 10 s^{-1} [18].Since NADH is a very expensive reducing agent(~$1000/mol), recycling it is essential for the process to be cost-effective[19]. Regenerating NADH from NAD^+ will also help drive the thermodynamically unfavorable reaction towards product formation (*i.e.*, formate and NAD^+), thereby improving reaction yields[11, 13, 20, 21]. Therefore, efficient regeneration of NADH is essential for the in-vitro CO_2 fixation process to be economically feasible. Regeneration/recycling of NADH by the reduction of NAD^+ using a second enzyme, electrochemically or photochemically has been reported[19]. However, the missing step in the overall process is an O_2-tolerant and robust enzyme to catalyze the in-vitro CO_2 fixation.

In this study, we report a highly thermodynamically efficient and cost-effective biocatalytic process for the transformation of CO_2 to formic acid using a formate dehydrogenase (FdsABG) from *C. necator.* Importantly, we cloned the full-length enzyme

and expressed it in *E. coli* with a His-tag fused to the N-terminus of the FdsG subunit. We analyzed the recombinant protein by electron paramagnetic resonance (EPR) spectroscopy and kinetic analysis and compared it with the native isolated FdsABG from *C. necator*. Finally, we combined this engineered *C. necator* FdsABG with a commercially available glucose dehydrogenase (Sigma-Aldrich) to promote continuous electron transfer to the reaction in which CO_2 is converted to formate. The results indicate that our engineered *C. necator* FdsABG has a total turnover number (TTN) of 1.9, which is the highest reported value for all FDHs [21]. This finding shows that the engineered *C. necator* FdsABG has the potential to be further developed for industrial applications.

3.3 Materials and Methods

3.3.1 Materials

All molecular cloning enzymes including Q5 DNA polymerase, T4 DNA ligase, BamHI and KpnI, were purchased from NEB. Glucose dehydrogenase (from *Pseudomonas sp*.), NAD^+ and NADH were purchased from Sigma-Aldrich (St. Louis, MO), Argon and CO_2 were procured from Airgas. Other chemicals were purchased from Fisher Scientific.

3.3.2 Cloning

FdsGBACD gene (Gene ID 4248878-4248882) was amplified by polymerase chain reaction (PCR) using *Cupriavidus necator* chromosomal DNA as template with respective primers (primer 1, 2 in Table 1). The 6xHis tag and Xpress Epitope from original pTrcHisB vector were replaced by a 6xHis-linker-6xHis tag using PCR with respective primers

(primer 3, 4 in SI. Table 1) to construct a new vector, pTrc12HLB. The PCR amplified pTrc12HLB DNA fragments were gel-purified, digested with BamHI, and ligated using T4 DNA ligase; the amplified FdsGBACD DNA fragment was gel-purified, digested with BamHI/KpnI, and cloned into both pTrcHisB and pTrc12HLB vector to encode 6xHis tag and 6xHis-linker-6xHis tag fused to the N-terminus of the fdsG subunit, respectively. ThepTrc12HLB-fdsGBACD vector was transformed into *Escherichia coli* DH5alpha cells for protein expression and purification.

Table 3.1 Summarized the primers in cloning work

Primer name	DNA sequence
Primer 1	5'- CTA GTG GAT CCG CCA GAA ATT TCC CCC CAC GCA CCG -3'
Primer 2	5'- ACG ATG GTA CCC TAC TCC AGC ATC GCC CGA TGC C -3'
Primer 3	5'- TAT CGA TTA AAT AAG GAG GAA TAA ACC ATG GGT GGA AGC CAC CAC CAC CAC CAC CAC TCT CGG GCT TGG AGA CAT CCT CAA GGG GGT TCT CAT CAC CAC CAC CAT CAC GGG ATG CGG GAT TTA TAT GAT GAC GAT GAC AAG GAT CCA GTC -3'
Primer 4	5'- TCT AAG GAT CCG AGC TCG AGA TCT -3'

3.3.3 Protein expression and purification

FdsGBACD was expressed in *E. coli* DH5alpha cells transformed with pTrc12HLB-fdsGBACD vector. Cells were pre-cultured at 37˚C for 7 hours in 3 mL LB medium containing 50 μg/mL ampicillin. The pre-cultures (200 μl) were transferred into 5 ml of LB containing 0.5 mM sodium molybdate and 50 μg/mL ampicillin and grown overnight at 28˚C with shaking. The cells were then inoculated into 2 L Terrific Broth (TB) medium supplemented with 50 μM isopropyl β-D-1-thiogalactopyranoside (IPTG), 1 mM sodium molybdate and 50 μg/mL ampicillin and grown additionally for 20–24 h at 28˚C

and 160 rpm. Cells were harvested at OD_{600} = 4.2-4.5 by centrifugation for 15 min at 5,000 x g and stored at -80˚C.

All protein purification steps were performed at 4˚C. The harvested *E. coli* cells were resuspended in 40 mM K-PO_4, 10 mM KNO_3, pH 7.2, containing 1 mM benzamidine, 1 mM sodium fluoride, 0.5 mM PMSF, lysozyme and Dnase I and disrupted by one passage through a French pressure cell at 10,000 psi. Cell supernatant was collected by centrifugation for 45 min at 150,000 x g, followed by a 25% saturation in ammonium sulfate, and centrifugation for an additional 45 min. The supernatant collected from the 25% fraction was then brought to 50% ammonium sulfate saturation and the pellet subsequently recovered by centrifugation for 20 min at >10,000 x g. The pellet containing FdsABG was then dissolved in 50 mM K-PO_4, 10 mM KNO_3 and 15 mM imidazole buffer, pH 7.5, containing 1 mM benzamidine, 1 mM sodium fluoride and 0.5 mM PMSF. The resuspended solution was batched with Ni-NTA agarose (Qiagen) for 1 h. The resin was then washed with 5-column volume of 50 mM K-PO_4, 10 mM KNO_3 and 20 mM imidazole buffer, pH 7.5, followed by 4 more washes with 5-column volume each of 50 mM K-PO_4, 10 mM KNO_3 and 30 mM imidazole buffer, pH 7.5. The bound protein was eluted with 5-column volume of 50 mM K-PO_4, 10 mM KNO_3 and 300 mM imidazole buffer, pH 7.5. The fractions containing FdsABG were then concentrated and loaded onto a Superdex 200 column (GE Healthcare). Size exclusion chromatography primarily separates the FdsABG from the FdsBG (also synthesized during induction of plasmid)[22]. Sample purity was confirmed with SDS-PAGE. Routine activity assays were performed as previously described[17, 18] at 30˚C in 75 mM K-PO_4, pH 7.7 with 2 mM NAD^+ and 40 mM sodium

formate. Enzyme concentrations were determined using an estimated extinction coefficient at 410 nm of 51,500 M^{-1} cm^{-1} for the oxidized enzyme spectrum[17, 23] and activities were calculated with respect to one trimer with a molecular weight of 178,800 Da[17, 18].

3.3.4 Protein characterization with EPR Spectroscopy

Mo-containing sample was prepared as previously described[17]. Electron paramagnetic resonance (EPR) spectra were recorded using a Bruker EMX spectrometer equipped with a Bruker ER 4119HS high sensitivity X-band cavity operating WinEPR version 4.33 acquisition software. Temperature was controlled using a Bruker variable temperature unit and liquid nitrogen cryostat. Simulations were performed as previously described[17].

3.3.5 Enzymatic reaction assay

Kinetic assays for FdsABG with formate and NAD^+ as substrate were performed under aerobic conditions at 30˚C as previously described[17]. To measure the steady-state parameters for the reaction of FdsABG with formate, 75 mM K-PO_4, pH 7.7 buffer was used for maintaining the pH. 4 mM formate with a range of 0 – 1 mM NAD^+, or 1 mM NAD^+ with a range of 0-3 mM formate were used in these assays and the results were plotted according to the Michaelis-Menten equation for calculating the k_{cat} values. The kinetic activity of glucose dehydrogenase (GDH) from *Pseudomonas sp*. was measured in 0.1 M phosphate buffer (pH 7.0) at 30˚C supplemented with 40 mM glucose with a range of 0-2.5 mM NAD^+, or 2 mM NAD^+ with a range of 0-40 mM glucose. Reactions were

initiated by addition of 5 nM GDH in 200 µl assays, and the first 60 sec after addition of GDH and the first 10 sec after addition of fdsABG were used to calculate the initial slopes. The rates of NADH consumption (for fdsABG) or generation (for GDH) were monitored at using a UV-vis spectrophotometer at 340 nm (ε= 6,220 M^{-1} cm^{-1}). The results were plotted according to the Michaelis-Menten equation for calculating the k_{cat} values.

To monitor the synthesis of formate from CO_2, enzyme cascade reactions in solution were employed. A 20 mL solution containing 20 mM bis-tris propane buffer, 4-50 mM glucose and 0.5 mM NAD^+ was first saturated with CO_2 and brought to pH 7.0. The reaction was started with injection of GDH and fdsABG at 1:20 ratio with an argon-purged gastight syringe. The reactions were incubated at 30˚C in a water bath with constant mixing. Samples at different time points were removed and the enzyme promptly separated via ultra-filtration with Amicon Ultra 4 (Millipore). The filtrate was analyzed by ion chromatography to quantify the amount of formate produced.

3.3.6 Formic Acid Detection Assay

The reaction samples were analyzed by ion chromatography (Dionex DX-120), using a 4 X 25 mm DionexIonpac AS22 column and 4.5 mM sodium carbonate/1.4 mM sodium bicarbonate as eluent with flow rate of 0.86 mL/min. A range of 0-2 mM formic acid dissolved in 20 mM bis-tris propane buffer supplemented with 20 mM glucose was used as standard for calibration.

3.4 Results and discussion

3.4.1 Protein expression and purification from *E. coli*

In our recent work [17, 18], FdsABG has only been purified from the bacterium *C. necator*. The culturing process of *C. necator* is very complex and time-consuming, requiring about 4 days of pre-culture, 6 hours of mass culture, followed by 2 days of large volume fermentation. Additionally, the FdsABG purification process is also very time-consuming, labor-intensive and expensive. Thus, in this study, we have constructed an overexpression system for the soluble *C. necator* fdsABG in *E. coli* to simplify both cell growth and protein purification. Purification was simplified via addition of an affinity histidine-tag at the N-terminus of FdsG. However, protein expression and purification still remained a challenge it two respects: synthesis and insertion of complex protein cofactors during expression and low protein binding affinity to Ni-NTA resin.

We first expressed FdsABG with 6xHis tag fused to the N-terminus of the fdsG subunit. We found that the soluble FdsABG was expressed by the *E. coli* recombinant system by monitoring the formate/NADH activity of the supernatant. However, the FdsABG protein was not able to bind to the Ni-NTA resin. We monitored the purification process utilizing a 1 ml HisTrap FF column and an Akta FPLC (GE Healthcare) at 280 nm for total protein quantification and at 450 nm, where FdsABG absorbs[17]. The chromatograms showed that much of the 6xHis-fdsABG was eluted from the Ni-NTA column with washing buffer containing only 20 mM imidazole (Figure 3.1A). We were additionally able to confirm the low column binding affinity by standard kinetic activity assay by comparing the activity of the cell lysate with the flow-through, the wash and the

elution fractions. As has been reported previously, a double-hexa-histidine (6xHis-linker-6xHis) tag, connecting two 6xHis tag with an intervening 11-amino acid linker, shows stronger binding to Ni-NTA surface than a conventional single 6xHis tag [24]. Therefore, we cloned a pTrc12HLB-fdsGBACDvector to encode FdsABG with a double-hexa-histidine(6xHis-linker-6xHis) tag fused to the N-terminus of the fdsG subunit. The affinity chromatography results (Figure 3.1A) showed that the protein with the 6xHis-linker-6xHis remained on the Ni-NTA column with washing buffer containing 20 mM imidazole and the protein eluted at >100 mM imidazole.

As previous studies have found for the homologous FdsABG from *R. Capsulatus*, heterologous expression not only results in the synthesis of the hexameric FdsABG but in addition the dimeric so-called "diaphorase subunit," FdsBG [22]. We found that this was indeed the case for the *C. necator* system as well and both FdsABG and FdsBG were expressed during induction of the plasmid with IPTG. Thus, the two proteins needed to be separated by size exclusion chromatography, using the Superdex 200 (GE Healthcare). After protein purification with Ni-NTA column, the fractions containing FdsABG were concentrated and loaded onto the size exclusion column. The resulting chromatograph (Figure 3.1B) showed three major peaks which correspond to a homodimer of trimers fdsABG $(\partial\beta\gamma)_2$ with a molecular mass of 358 kDa, a monomer of trimers fdsABG ($\partial\beta\gamma$) with a molecular mass of 179 kDa, and the fdsBG ($\beta\gamma$) dimer with a molecular mass of 74 kDa. The fractions containing the three major peaks from the size exclusion chromatography were subjected to denaturing SDS-PAGE (Figure 3.1B). Three major

bands were detected: 105 kDa, 55 kDa and 19 kDa, corresponding to subunits FdsA, FdsB and FdsG, respectively.

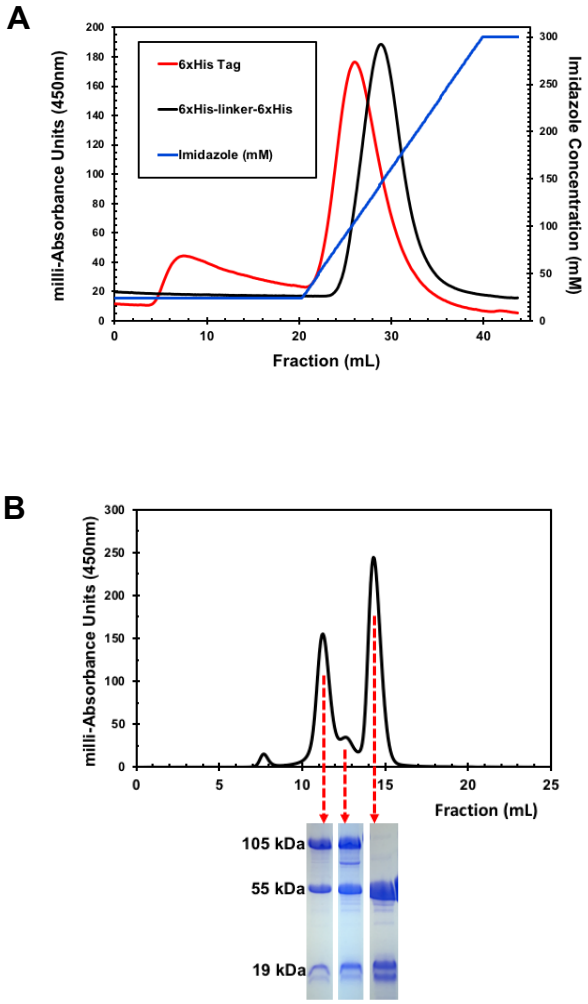

Figure 3.1 *FdsABG purification from E. coli: (A) Affinity chromatography and purification of 6xHis-fdsABG (red line) and 6xHis-linker-6xHis-fdsABG (black line) on a Ni-NTA column. The 6xHis-fdsABG showed a first peak from a washing step of 20 mM imidazole and a second peak from a gradient elution of 20-300 mM imidazole (blue line), whereas the 6xHis-linker-6xHis-fdsABG eluted with only one peak at >100 mM imidazole. (B) Size-exclusion chromatography and purification of 6xHis-linker-6xHis-fdsABG were performed after Ni-NTA affinity purification. The fractions from each eluted protein peak were collected and concentrated, and further analyzed on a 15% denaturing SDS-PAGE. All purification processes were monitored by FdsABG absorbance at 450 nm.*

To optimize the level of active FdsABG expression, *E. coli* DH5alpha cells transformed with pTrc12HLB-fdsGBACD vector were cultured under different growth conditions. In general, higher IPTG concentrations and faster growth (as a result of either higher shaking speeds and/or higher temperatures) favored the synthesis of FdsBG. The level of Molybdenum cofactor (MGD) saturation is also affected by temperature, oxygen tensor and IPTG concentrations [22]. In general, slower cell growth attained by low shaking speeds and lower temperature in combination with low IPTG concentrations for slower protein expression rates favors higher MGD cofactor saturation.

3.4.2 Protein characterization with EPR spectroscopy

We next examined the EPR properties of the recombinant form of FdsABG in order to verify that the addition of the 6xHis-linker-6xHis tag fused to the N-terminus of the FdsG subunit did not perturb the structure of FdsA subunit by probing the magnetic properties of the Mo-cofactor contained within. To that end, a Mo^{V} intermediate was generated as previously described [17]: The enzyme was partially reduced with sodium dithionite under anaerobic conditions and promptly frozen for EPR analysis. The resultant spectrum is presented in Figure 3.2A (black trace) with the corresponding simulation below (red trace). For comparison the spectrum (black trace) and simulation (blue trace) for the native FdsABG are shown in Figure 3.2B (reprinted by permission[17]). The spectrum of the recombinant protein is composed of a narrow feature centered around 338 mT belonging to the Mo^{V} species, including the 25% naturally occurring [95,97] Mo (I=5/2) hyperfine splittings and a broad signal attributed to one of the seven Fe/S clusters present in FdsABG

(the only Fe/S signal that is observed at 150 K, the temperature at which the data was collected). Simulation of the composite Mo^{V}-Fe/S spectrum yielded identical g-values as well as near identical proton splittings for the Mo^{V} contribution to the spectrum (the Mo^{V} hyperfine splittings were fixed during this simulation) indicating that the Mo-center was not perturbed by the addition of the 6xHis-linker-6xHis tag. The g-values for the Fe/S component of the composite spectrum were also in excellent agreement with the values obtained for the native FdsABG.

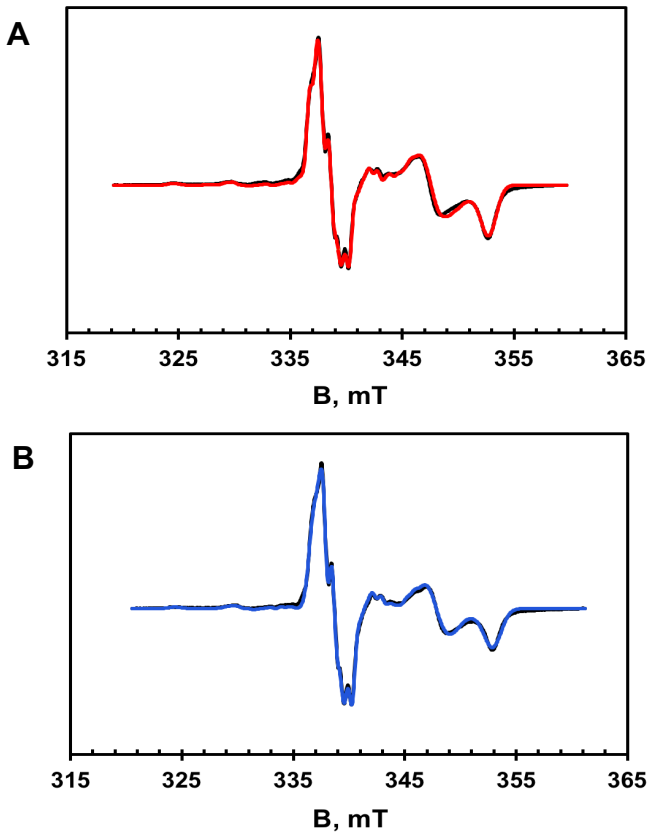

Figure 3.2 *EPR spectroscopy of Mo-center of FdsABG: (A) EPR spectrum (black trace) and simulation (red trace) of recombinant FdsABG (B) EPR spectrum (black trace) and simulation (red trace) of native FdsABG. (Reprint by permission[17])*

3.4.3 Protein characterization with kinetic assays

In this study, we have also characterized the recombinant FdsABG with kinetic assays and compared it with the native, isolated FdsABG from *C. necator*. The native, isolated FdsABG from *C. necator* is a homodimer of trimers, $(\partial\beta\gamma)_2$, in which the 105 kDa ∂ (FdsA) subunit contains a molybdenum center (bis-MGD), four [4Fe-4S] clusters and a [2Fe-2S] cluster; the 55 kDa ß (FdsB) subunit contains a flavin (FMN) cofactor and a [4Fe-4S] cluster; finally, the 19 kDa γ (FdsG) subunit contains one [2Fe-2S]. Figure 1.2 from chapter 1 shows the architecture of FdsABG. In this complex, the active site molybdenum center (bis-MGD) is the reaction center responsible for the interconversion of CO_2 and formate. The seven iron-sulfur clusters are responsible for the electron transfer within the protein, and the FMN is the site of NAD^+ reduction. The loss of any one of these cofactors during the expression and purification process, results in the loss of enzymatic activity as measured by either the formate/NAD^+ or the CO_2/NADH kinetic assays. Therefore, we have used the steady-state kinetic properties of the native, isolated FdsABG from *C. necator* as the standard for characterizing the activity of the recombinant protein[17, 18]. The recombinant FdsABG yielded a k_{cat} for formate oxidation of 99 s^{-1} and a k_{cat} for CO_2 reduction of 4.8 s^{-1} under the same experimental conditions as those used for the native enzyme (Figure 3.3 and Figure 3.7) [17]. By comparing these results with those for the native FdsABG from *C. necator (*k_{cat}= 11 s^{-1} for CO_2 reduction and k_{cat}= 201 s^{-1} for formate oxidation) we demonstrate that the recombinant FdsABG has been successfully expressed and purified with about 50% functionality. This value is in good agreement with

heterologous expression of other MGD cofactor containing enzymes and typically reflects the cofactor saturation of the enzyme [22].

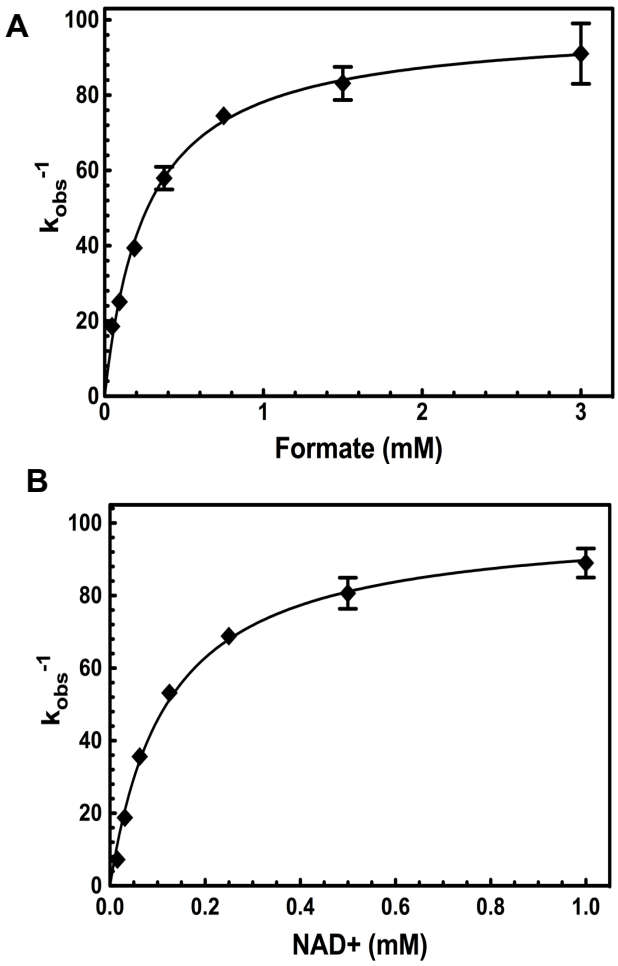

Figure 3.3 *Steady-state kinetic properties of recombinant FdsABG* ***(A)*** *Hyperbolic plots for the reaction of FdsABG with formate at 1 mM NAD^+.* ***(B)*** *Hyperbolic plots for the reaction of FdsABG with NAD^+ at 4 mM formate. Reactions in (A) and (B) yielded a $K_m^{formate}$ = 260 µM and a $K_m^{NAD^+}$ = 110 µM, respectively and an average k_{cat} of 99 s^{-1}. All reactions were performed in 75 mM K-PO_4, pH 7.7 at 30˚C under aerobic conditions.*

3.4.4 Production of formate with fixation of CO_2 based on enzymatic regeneration of NADH

The biotechnology sector and energy sector have brought great attention to utilizing formate dehydrogenase (FDH) to catalyze CO_2 to formate, as this solves two problems, excess emission of CO_2 and depletion of fossil fuels, in a single process. However, the major challenge in working with most FDHs is their intolerance to O_2 and low turnover rates in catalyzing the *in vitro* CO_2 fixation. To extend the analysis of the ability of the recombinant FdsABG to catalyze CO_2 to formate, we have combined FdsABG with a glucose dehydrogenase (GDH) in a cascade reaction; Figure 3.4 presents the schematic for this process. The enzyme GDH catalyzes the oxidation of glucose to gluconolactone and in the process generates two protons and two electrons, which are used to reduce NAD^+ to NADH (Eq.3.1), and subsequently fdsABG

$$\beta\text{-D-glucose} + NAD^+ \rightarrow \text{D-}\delta\text{-gluconolactone} + NADH + H^+ \qquad \text{(Eq. 3.1)}$$

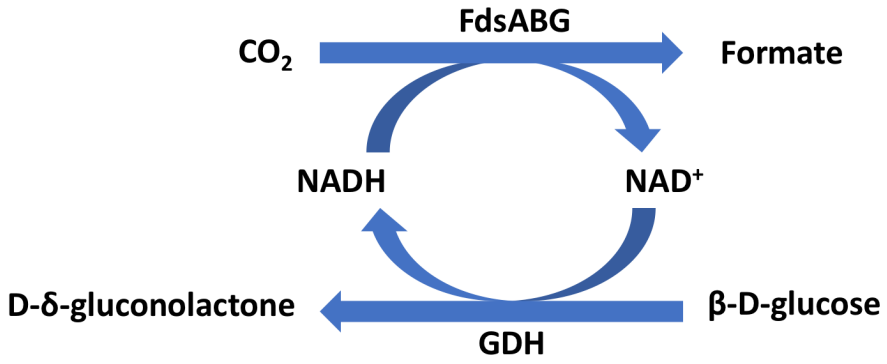

Figure 3.4 *Schematic illustration of enzymatic cascade reaction involving FdsABG and GDH: FdsABG catalyzes the conversion of carbon dioxide to formic acid, while NADH is oxidized to NAD^+. GDH catalyzes the conversion of β-D-glucose to D-δ-gluconolactone, while NAD^+ from FdsABG reaction is reduced to NADH.*

To investigate the suitability of GDH for the cascade reaction, we first performed a steady-state analysis of the enzyme under the optimum reaction conditions for the recombinant FdsABG (30˚C, 1 atm, pH 7.0). As shown in Figure 3.5, the results were plotted according to the Michaelis-Menten equation and yielded hyperbolic relationships from which kinetic parameters could be extracted. A k_{cat} of 200 s^{-1} and a $K_m^{glucose}$ of 2.7 mM (Figure 3.5a) and a $K_m^{NAD^+}$ of 120 µM at pH 7.0 (Figure 3.5b) were thus obtained.

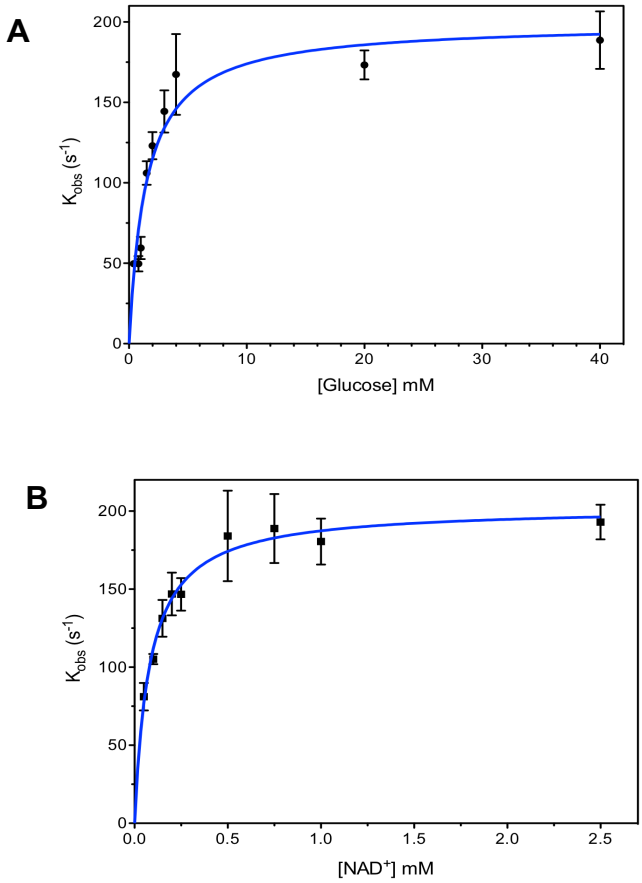

Figure 3.5 *Steady-state kinetic properties of GDH* ***(A)*** *Hyperbolic plots for the reaction of GDH with glucose at 2 mM NAD^+.* ***(B)*** *Hyperbolic plots for the reaction of FdsABG with NAD^+ at 40 mM glucose. Reactions in (A) and (B) yielded a $K_m^{glucose}$ = 2.7 mM and a $K_m^{NAD^+}$ = 120 µM, respectively and an average k_{cat} of 200 s^{-1}. All reactions were performed in 100 mM K-PO_4, pH 7.0 at 30˚C under anaerobic conditions.*

Next, we combined GDH and FdsABG in a ratio which reflects similar activities (based on k_{cat} values at pH 7.0) to promote continuous electron transfer for the reaction in which CO_2 is converted to formate. As shown in Figure 3.6, in one group of experiments (blue squares), we used substrate concentrations that were saturating for both enzymes: 20mM glucose, 0.5 mM NAD^+ and 28 mM dissolved CO_2 gas at 30˚C, 1 atm, pH 7.0. Samples were removed at different time points after addition of both FdsABG and GDH and formate was quantified by ion chromatography. We found that formate accumulated quickly after the reaction was initiated but the rate would slow down dramatically after 4 hours. Additionally, the formate concentration stalled at 1 mM even after 10 hours of reaction time. There are a number of possible reasons for the reaction plateau including enzyme inactivation, substrate limitation and production inhibition of FdsABG. To distinguish between these possibilities, we performed several reactions and steady-state experiments whose results are presented in Figure 3.6 and Figure 3.7. To test for the inactivation of one or both of the enzymes during the progress of the 10-hour reaction, a similar amount of GDH and FdsABG was introduced at 2 hours after the reaction was started (Figure 3.6, green triangles). Additional enzyme, however, only marginally improved the production of formate; maximum concentration still did not exceed 1.1 mM. We also tested the effect of varying the glucose concentration on the yield of formate after a 10-hour reaction period. Under the conditions of saturated CO_2 (28 mM) and NAD^+ (0.5 mM), 4 mM of glucose yielded only 0.2 mM formate (Figure 3.6, pink squares), while increasing glucose to 50 mM (Figure 3.6, red squares), did not yield any more formate than 20 mM glucose used in the previous experiments. We also decreased the NAD^+

concentration to 0.2 mM (Figure 3.6, yellow squares), under the same conditions as above with a result that formate production decreased to 0.7 mM after the 10-hour incubation. Finally, we performed a series of steady-state experiments with a saturated solution of CO_2 and 0.2 mM NADH in the presence of 0-1.5 mM formate to test for product inhibition of FdsABG (Figure 3.7). The data indicated that the k_{cat}^{CO2} was dramatically affected by the presence of formate, decreasing to 22% in the presence of 1.5 mM of the product. The implication of the above experiments is that product inhibition is the major reason for the rate decreases and eventual stagnation in the yield of formate in the cascade reaction. Thus, for production of formate with FdsABG at maximum rate, the product would need to be continuously removed to a level below 0.4 mM for maintaining the reaction of CO_2 reduction catalyzed by FdsABG at relative high rate. According to the reaction scheme in Figure 3.4, 1 mol NADH will be consumed to produce 1 mol of formate. Based on this stoichiometry, we can calculate the NADH-based formate yield according to the following equation (Eq. 3.2).

$$Y_{\mathrm{formate,t}}(\%) = \frac{C_{\mathrm{formate,t}}}{C_{\mathrm{NADH,initial}}} 100 \qquad \text{(Eq. 3.2)}$$

The NADH-based formate yield of the reaction was calculated based on percentage of formate production concentration (0.9 mM) divided by the initiation concentration of NADH (0.5 mM). The total yield is about 190%, which corresponds to a total turnover number (TTN) of NADH is about 1.9. In comparison to previous studies on FDHs [9, 21], the results indicate that our engineered *C. necator* FdsABG is a robust enzyme for CO_2 reduction to formate with the highest TTN 1.9 reported value for all.

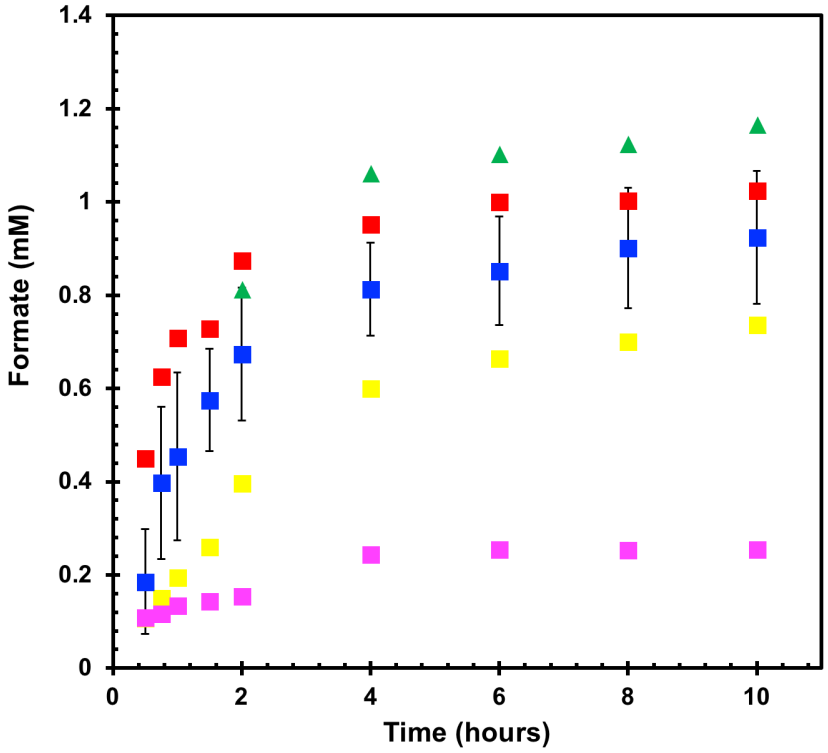

Figure 3.6 *Plots of formate production as a function of reaction time for enzymatic cascade reaction involving FdsABG and GDH. Reactions of FdsABG and GDH with 28 mM dissolved CO_2 gas, 0.5 mM NAD^+ and 20 mM glucose (■), or 4 mM of glucose (■), or 50 mM glucose (■). Additional enzymes were introduced to blue square group at 2 hours after the reaction was started (▲). Reactions of FdsABG and GDH with 28 mM dissolved CO_2 gas, 0.2 mM NAD^+ and 20 mM glucose (■). All reactions were measured by ion chromatography for the change in formate, and all reactions were performed in 20 mM Bis-tris buffer at pH 7.0 and 30˚C.*

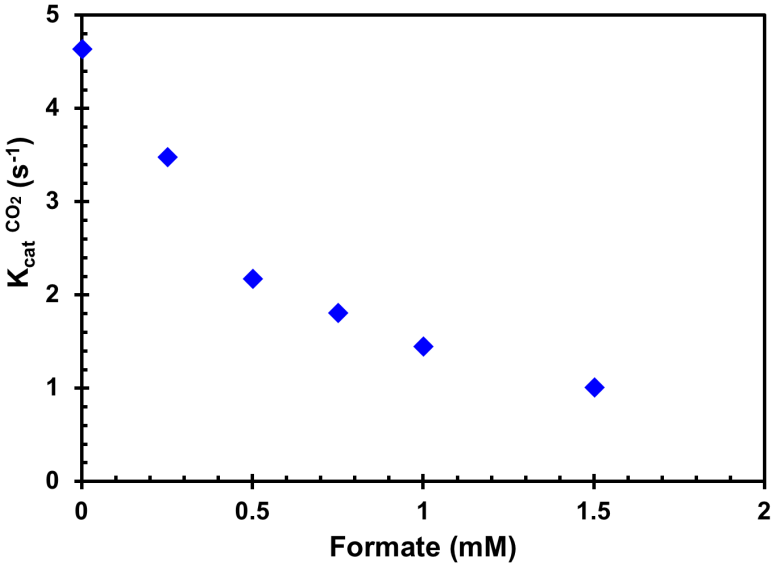

Figure 3.7 *The inhibition effect of formate concentration on the reaction of FdsABG on with 200 µM NADH and saturated (28 mM) CO_2(aq). The reaction of recombinant FdsABG with CO_2 and no initial formate yield a $k_{cat}^{CO_2}$ of 4.7 s^{-1}, As the initial concentration of formate increase, the $k_{cat}^{CO_2}$ for recombinant FdsABG drop. All reactions were performed in 100 mM K-PO_4 Buffer at pH 7.0 and 30˚C under anaerobic conditions.*

3.5 Conclusion

In this study, we have successfully cloned the full-length soluble formate dehydrogenase (FdsABG) from *C. necator* and heterologous-expressed and purified from *E. coli* with a 6xHis-linker-6xHis tag fused to the N terminus of fdsG subunit. We have also characterized the recombinant fdsABG with EPR spectroscopy as well as kinetic assays and compared it with the native, isolated FdsABG from *C. necator.* As expected, the recombinant FdsABG has about 50% functionality compared with the native isolated one.

We have further combined this recombinant *C. necator* FdsABG with another biological enzyme, Glucose Dehydrogenase, for continuous electron donation to the reaction of converting CO_2 to formate. The results showed that our engineered *C. necator* FdsABG has a highly thermodynamic efficient to the reduction of CO_2 process with a total turnover number of 1.9. The present work showed that the recombinant *C. necator* fdsABG has a great potential for industrial applications because of its air-stable and high TTN properties, and perspective development of increasingly efficient biocatalytic processes for CO_2 fixation. Importantly, the present work also provides a framework of studying electron transfer mechanisms inside this protein as well as applications for a highly efficient CO_2 biocatalytic fuel-cell.

3.6 Reference

1. Appel, A. M.; Bercaw, J. E.; Bocarsly, A. B.; Dobbek, H.; DuBois, D. L.; Dupuis, M.; Ferry, J. G.; Fujita, E.; Hille, R.; Kenis, P. J. A.; Kerfeld, C. A.; Morris, R. H.; Peden, C. H. F.; Portis, A. R.; Ragsdale, S. W.; Rauchfuss, T. B.; Reek, J. N. H.; Seefeldt, L. C.; Thauer, R. K.; Waldrop, G. L., Frontiers, Opportunities, and Challenges in Biochemical and Chemical Catalysis of CO_2 Fixation. Chemical Reviews 2013, 113 (8), 6621-6658.

2. Enthaler, S.; von Langermann, J.; Schmidt, T., Carbon dioxide and formic acid-the couple for environmental-friendly hydrogen storage? Energy & Environmental Science 2010, 3 (9), 1207-1217.

3. Sordakis, K.; Tang, C. H.; Vogt, L. K.; Junge, H.; Dyson, P. J.; Beller, M.; Laurenczy, G., Homogeneous Catalysis for Sustainable Hydrogen Storage in Formic Acid and Alcohols. Chemical Reviews 2018, 118 (2), 372-433.

4. Yadav, M.; Xu, Q., Liquid-phase chemical hydrogen storage materials. Energy & Environmental Science 2012, 5 (12), 9698-9725.

5. Shi, J. F.; Jiang, Y. J.; Jiang, Z. Y.; Wang, X. Y.; Wang, X. L.; Zhang, S. H.; Han, P. P.; Yang, C., Enzymatic conversion of carbon dioxide. Chemical Society Reviews 2015, 44 (17), 5981-6000.

6. Zhong, H.; Iguchi, M.; Chatterjee, M.; Himeda, Y.; Xu, Q.; Kawanami, H., Formic Acid-Based Liquid Organic Hydrogen Carrier System with Heterogeneous Catalysts. Advanced Sustainable Systems 2018, 2 (2).

7. Qiao, J.; Liu, Y.; Hong, F.; Zhang, J., A review of catalysts for the electroreduction of carbon dioxide to produce low-carbon fuels. Chemical Society Reviews 2014, 43 (2), 631-675.

8. Maia, L. B.; Moura, J. J. G.; Moura, I., Molybdenum and tungsten-dependent formate dehydrogenases. Journal of Biological Inorganic Chemistry 2015, 20 (2), 287-309.

9. Maia, L. B.; Moura, I.; Moura, J. J. G., Molybdenum and tungsten-containing formate dehydrogenases: Aiming to inspire a catalyst for carbon dioxide utilization. Inorganica Chimica Acta 2017, 455, 350-363.

10. Choe, H.; Joo, J. C.; Cho, D. H.; Kim, M. H.; Lee, S. H.; Jung, K. D.; Kim, Y. H., Efficient CO_2-Reducing Activity of NAD-Dependent Formate Dehydrogenase from Thiobacillus sp KNK65MA for Formate Production from CO_2 Gas. Plos One 2014, 9 (7).

11. El-Zahab, B.; Donnelly, D.; Wang, P., Particle-tethered NADH for production of methanol from CO_2 catalyzed by coimmobilized enzymes. Biotechnology and Bioengineering 2008, 99 (3), 508-514.

12. Yadav, R. K.; Baeg, J.-O.; Oh, G. H.; Park, N.-J.; Kong, K.-j.; Kim, J.; Hwang, D. W.; Biswas, S. K., A Photocatalyst-Enzyme Coupled Artificial Photosynthesis System for Solar Energy in Production of Formic Acid from CO_2. Journal of the American Chemical Society 2012, 134 (28), 11455-11461.

13. Kim, S.; Kim, M. K.; Lee, S. H.; Yoon, S.; Jung, K.-D., Conversion of CO_2 to formate in an electroenzymatic cell using *Candida boidinii* formate dehydrogenase. Journal of Molecular Catalysis B-Enzymatic 2014, 102, 9-15.

14. Srikanth, S.; Maesen, M.; Dominguez-Benetton, X.; Vanbroekhoven, K.; Pant, D., Enzymatic electrosynthesis of formate through CO_2 sequestration/reduction in a bioelectrochemical system (BES). Bioresource Technology 2014, 165, 350-354.

15. de Bok, F. A. M.; Hagedoorn, P. L.; Silva, P. J.; Hagen, W. R.; Schiltz, E.; Fritsche, K.; Stams, A. J. M., Two W-containing formate dehydrogenases (CO_2-reductases) involved in syntrophic propionate oxidation by *Syntrophobacter fumaroxidans*. European Journal of Biochemistry 2003, 270 (11), 2476-2485.

16. Oh, J. I.; Bowien, B., Structural analysis of the fds operon encoding the NAD($^+$)-linked formate dehydrogenase of *Ralstonia eutropha*. Journal of Biological Chemistry 1998, 273 (41), 26349-26360.

17. Niks, D.; Duvvuru, J.; Escalona, M.; Hille, R., Spectroscopic and Kinetic Properties of the Molybdenum-containing, NAD($^+$) - dependent Formate Dehydrogenase from *Ralstonia eutropha*. Journal of Biological Chemistry 2016, 291 (3), 1162-1174.

18. Yu, X. J.; Niks, D.; Mulchandani, A.; Hille, R., Efficient reduction of CO_2 by the molybdenum-containing formate dehydrogenase from *Cupriavidus necator* (*Ralstonia eutropha*). Journal of Biological Chemistry 2017, 292 (41), 16872-16879.

19. Weckbecker, A.; Groeger, H.; Hummel, W., Regeneration of Nicotinamide Coenzymes: Principles and Applications for the Synthesis of Chiral Compounds. Biosystems Engineering I: Creating Superior Biocatalysts 2010, 120, 195-242.

20. Addo, P. K.; Arechederra, R. L.; Waheed, A.; Shoemaker, J. D.; Sly, W. S.; Minteer, S. D., Methanol Production via Bioelectrocatalytic Reduction of Carbon Dioxide: Role of Carbonic Anhydrase in Improving Electrode Performance. Electrochemical and Solid State Letters 2011, 14 (4), E9-E13.

21. Ji, X.; Su, Z.; Wang, P.; Ma, G.; Zhang, S., Tethering of Nicotinamide Adenine Dinucleotide Inside Hollow Nanofibers for High-Yield Synthesis of Methanol from Carbon Dioxide Catalyzed by Coencapsulated Multienzymes. Acs Nano 2015, 9 (4), 4600-4610.

22. Hartmann, T.; Leimkuehler, S., The oxygen-tolerant and NAD(+)-dependent formate dehydrogenase from *Rhodobacter capsulatus* is able to catalyze the reduction of CO_2 to formate. Febs Journal 2013, 280 (23), 6083-6096.

23. Khan, F.; He, M. Y.; Taussig, M. J., Double-hexahistidine tag with high-affinity binding for protein immobilization, purification, and detection on Ni-nitrilotriacetic acid surfaces. Analytical Chemistry 2006, 78 (9), 3072-3079.

Chapter 4

Electrochemistry of the Mo-containing formate dehydrogenase from *Cupriavidus necator*

4.1 Abstract

Dynamic electrochemical studies of adsorbed enzyme on electrodes not only provide the electrons of the redox reaction, but also introduce the "potential dimension" into the enzyme kinetics and biocatalysis reaction. In this study, we have adsorbed FdsABG from *C. necator* on electrode and have studied dynamic electrochemistry of the enzyme. Unfortunately, we find that *C. necator* FdsABG has no direct electron response to the bioelectrochemical system. This may be associated with the complex structure of the *C. necator* FdsABG. FdsABG, however, can bioelectrochemically catalyze the reaction of interconverting CO_2 and formate using Methyl viologen (MV) as the electron transfer mediator. We further studied the kinetic parameters of the FdsABG on electrode for the reduction of CO_2 and confirmed that formate was the only product.

4.2 Introduction

As an abundant greenhouse gas, carbon dioxide not only causes serious problems to the environment and climate, but also poses challenges to the energy sector. The energy sector faces not only a shortage of fossil fuel, but about 9 giga tons of carbon dioxide a year from burning fossil fuels[1]. Therefore, a significant effort has been made to convert

carbon dioxide into energy[1-3]. Formate is considered a promising liquid fuel as a hydrogen energy carrier with advantages of high volumetric capacity (53 g H_2/L), low toxicity and flammability under ambient conditions[4-7]. Meanwhile, formate is also considered as an important feedstock to synthesize other valuable chemicals[4, 8]. An attractive solution is using biocatalysis to convert CO_2 into formate[7, 9]. Formate dehydrogenase (FDHs) is a category of enzymes that could catalyze such reactions. FDHs give these reactions a variety of advantages, including mild reaction conditions, room temperature under ambient pressure, and neutral pH[3].

Dynamic electrochemical studies of adsorbed FDHs on electrodes not only provide the electrons of the redox reaction, but also introduce the "potential dimension" into the enzyme kinetics and biocatalysis reaction. Several FDHs have been reported in dynamic electrochemical studies[10], including the W-dependent FDH from *Syntrophobacter fumaroxidans* (*Sf*FDH1)[11], and Mo-dependent FDH from *E. coli* (*Ec*FDH-H)[12]. *Sf*FDH1 is the first reported FDH, which can convert CO_2 and formate rapidly, specifically and reversibly under mild electrochemical reaction conditions through direct electron transfer mechanism[11]. Although SfFDH1 has a variety of catalytic advantages, it also has many thorny problems for practical applications. *Sf*FDH1 has a complex and large protein architecture: a 180 kDa heterotrimer containing one W active site and nine iron-sulfur clusters.[13] Furthermore, *Sf*FDH1 is difficult to express from its native anaerobic bacterium *Syntrophobacter fumaroxidans*[13]. The entire purification and culture process takes several months, and only minuscule amounts of oxygen sensitive protein was produced[11, 13]. Better than *Sf*FDH1, *Ec*FDH-H has a simple and relatively smaller protein structure, containing

only one Mo redox center and one iron-sulfur cluster[14]. At the same time, *Ec*FDH-H also has the advantages of easy purification from *E. coli*[15] and bidirectional bioelectrocatalysis of CO_2 and formate[12]. However, similar to *Sf*FDH1, *Ec*FDH-H is a highly oxygen sensitive enzyme because it contains a selenocysteine residue that is coordinated with the metal center.

Similar to *Sf*FDH1 and *Ec*FDH-H, formate dehydrogenase from *Cupriavidus necator* (FdsABG) is a prokaryotic metal-dependent FDH belonging to the DMSO reductase family[3, 16]. The difference is that FdsABG is a Mo-containing/NAD^+-dependent FDH with an advantage of O_2 tolerance, which is unusual among the metal-dependent FDHs family[3, 17-19]. Majority members from the metal-dependent FDHs family bear a selenocysteine residue at the metal center, and this residue causes enzyme to lose functionality shortly after exposure to oxygen[3]. Other than the O_2-tolerance property, FdsABG also has other beneficial properties including a high-water solubility and easy purification from *E. coli* recombinant system (from Chapter 3). The *C. necator FdsABG* is also a soluble homodimer complex of trimers, *i.e.*, $(\partial ß \gamma)_2$, in which each trimer contains seven iron-sulfur clusters as well as the bis (molybdopterin guanine dinucleotide) molybdenum (bis(MGD)Mo) cofactor and FMN[18-20]. Our previous studies have shown that FdsABG can effectively catalyze the reduction of CO_2 using NADH as a terminal electron donor with k_{cat} of 10 s^{-1} for native FdsABG[17], or 5 s^{-1} for recombinant FdsABG (from Chapter 3). However, NADH is a very expensive reducing agent (~$1000/mol). Therefore, recycling or excluding it is essential for the process to be cost-effective[21]. As described in

chapter 3, we have studied regenerating NADH from NAD^+ enzymatically and coupled with the recombinant FdsABG.

In this chapter, we studied the dynamic electrochemistry of the recombinant FdsABG adsorbed on electrodes. Importantly, we first examined this bioelectrocatalytic process by means of direct electron transfer (DET). Multiple carbon nanomaterials and different enzyme loadings were tested, but no catalytic wave was found. Next, we studied this bioelectrocatalytic process via mediated electron transfer (MET). We understood that FdsABG can catalyze the reversible reaction of interconverting CO_2 and formate with methyl viologen (MV) as the electron transfer mediator. Finally, we studied the kinetic parameters of the FdsABG on electrode for the reduction of CO_2 and confirmed that formate was the only product.

4.3 Materials and methods

4.3.1 *C. necator* FdsABG purification

In the previous study (chapter 3), we have cloned the full-length soluble formate dehydrogenase (FdsABG) from *C. necator* and heterologous-expressed in *E. coli* with a 6xHis-linker-6xHis tag fused to the N terminus of fdsG subunit. In this study, *E. coli* DH5alpha cells transformed with pTrc12HLB-fdsGBACD vector were grown as previously described (Chapter 3). In brief, cells were grown in 2 L Terrific Broth (TB) medium supplemented with 50 μM isopropyl β-D-1-thiogalactopyranoside (IPTG), 1 mM sodium molybdate and 50 μg/mL ampicillin at 28˚C and 160 rpm, and protein purification steps were performed at 0-4°C first with a Ni-NTA column and followed with a Superdex

200 column. After the purification steps, FdsABG was tested on SDS-PAGE and confirmed with routine activity assays under standard assay condition, 30˚C in 75 mM KH_2PO_4, pH 7.7 with 2 mM NAD^+ and 40 mM sodium formate[17, 19]. Enzyme concentrations were determined using an estimated extinction coefficient at 410 nm of 51,500 M^{-1} cm^{-1} and activities were calculated with respect to one trimer with a molecular weight of 178.8 kDa

4.3.2 Synthesis of multiwall carbon nanotubes (MWCNTs) buckypaper electrode

The procedure of fabrication of MWCNT buckypaper electrode was modified from a previous study[22]. Specifically, 120 mg of commercially available MWCNT powder (95 wt.% purity, outside diameter <8 nm, Nanointegris, Boisbriand, Canada) was suspended in 120 mL of N, N-dimethylformamide (DMF) and probe sonicated for 1 h. 60 mL of the suspension was filtered through a hydrophilic Polytetrafluoroethylene (PTFE) membrane (JHWP04700, 0.45 μm pore size, and OD=47 mm, Millipore Sigma, Massachusetts, US) using a vacuum filtration system. The MWCNTs were packed on top of the membrane as a thin paper film. The MWCNT buckypaper was washed with water and dried overnight at room temperature. The completely dried MWCNT buckypaper was then cut into electrodes of 1 cm diameter. The backside and the edge of the electrode were sealed with Polydimethylsiloxane (PDMS)at 100 ˚C for 1 h.

4.3.3 Enzyme electrode fabrication and electrochemical characterization

0.25 g of chitosan was dissolved in a 100 mL of 0.1 M acetate buffer at pH 5.0, resulting in a 0.25 wt.% chitosan solution. 20 mg of MWCNTs was then suspended in 5 mL of 0.25 wt.% chitosan solution and sonicated for 1 h. The MWCNT-chitosan nanocomposite modified glassy carbon electrodes (MWCNT-GCE) were prepared by drop casting 5 μL of the MWCNT-chitosan suspension on top of GCE (OD=3 mm). Prior to casting enzyme, the electrodes were electrochemically tested in 0.01 M $K_3[Fe(CN)_6]$, 0.1 M KCl solution by performing 10 cyclic voltammogram scans from −0.2 to +0.6 V at a scan rate of 50 mV/s. The FdsABG-MWCNT-chitosan electrodes (FdsABG-MWCNT-GCE) were prepared by drop casting the enzyme on top of the MWCNT-GCE electrode. For electrodes modified with rGO, the fabrication process is similar to that of MWCNT-GCE electrodes without chitosan. Specifically, 20 mg of rGO was suspended in 5 ml water and probe sonicated for 30 min, and then 5 μl of rGO suspension was drop casted on top of GCE electrode to be rGO-GCE electrodes. The enzyme-rGO composite electrodes were produced by direct casting enzyme on top of rGO-GCE electrodes. All enzyme electrodes were dried at 4˚C overnight and stored at 4˚C in 0.1 M K-PO_4, 20 mM KNO_3, pH 7.0 buffer for future use.

4.3.4 Formic Acid Detection by Ion Chromatography

Bulk electrocatalysis of CO_2 reduction with FdsABG_MWCNT_GCE electrodes was conducted in an electrolyte solution containing saturated CO_2 and 5 mM MV in 20 mM Bis-Tris propane (final pH 6.3, 25˚C). The reaction was followed by a reduction

current decrease at -800 mV *vs*. Ag/AgCl for 2 h. The final reaction samples from the bulk electrocatalysis were analyzed by ion chromatography (Dionex DX-120) using a DionexIonpac AS22 4 X 25 mm column and 4.5 mM sodium carbonate/1.4 mM sodium bicarbonate as eluent with a flow rate of 0.86 mL/min. A range of 0-2 mM formic acid dissolved in 20 mM bis-tris propane buffer supplemented with 5 mM MV was used for standard calibration.

4.4 Results and discussion

4.4.1 *C. necator* FdsABG has no direct electron transfer (DET) with electrode

Figure 4.1 illustrates a schematic of the bioelectrocatalytic process for the interconversion of CO_2 and formate by FdsABG on the electrode surface. To-date, the structure of *C. necator FdsABG* is still unknown, so the enzyme model shown in Figure 4.1 is a proposed architecture of a monomer of *C. necator* FdsABG (∂ßγ) from a prior study[20].

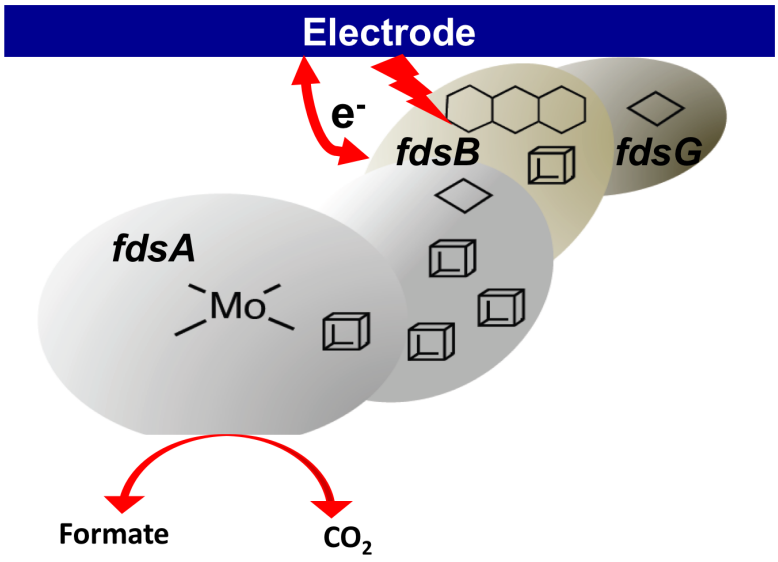

Figure 4.1. *A schematic illustration of a bioelectrocatalysis reaction of CO_2 reduction by an adsorbed FdsABG on electrode*

To achieve an efficient bioelectrocatalytic reaction, the entire process requires not only an active enzyme absorbed on the electrode surface, but also a large electroactive surface area to adsorb a large amount of enzyme, as well as a working electrode with high electrocatalytic activity materials for efficient communication between adsorbed enzyme and electrons[23-25]. Because of the complexity of *C. necator* FdsABG structure (shown in Figure 4.1), we first synthesized a buckypaper electrode with multiwall carbon nanotube (MWCNT) as the adsorbed electrode surface for *C. necator* FdsABG. MWCNT is a multi-layer concentric cylindrical carbon allotrope composed of sp^2 hybridized carbon atoms similar to graphite[26]. Meanwhile, MWCNT is a promising bioelectrode material with advantages including: a large surface area, a good stability and high conductivity[26]. MWCNT-based buckypaper electrode can provide a large electrode surface with easy

fabrication process[22, 27]. Multiple studies have shown that MWCNT is a great material for bioelectrode, which can improve the direct electron transfer between electrode and enzyme, *e.g.*, glucose oxidase[28, 29]. Therefore, we hypothesized that a MWCNT buckypaper working electrode would provide a large electrode surface as well as a high conductive surface to communicate with FdsABG. In contrast, results showed that unmodified MWCNT buckypaper electrode had a poor electrocatalytic property compared with glassy carbon electrode (GCE) (Figure 4.2). To further improve the stability and electrochemical properties of the MWCNT buckypaper electrode, modification is required, including addition of small electron transfer molecules, such as porphyrin and phenanthroline quinone (PLQ), or coating of MWCNT buckypaper film on the surface of a solid electrode, such as a glassy carbon electrode[22, 27].

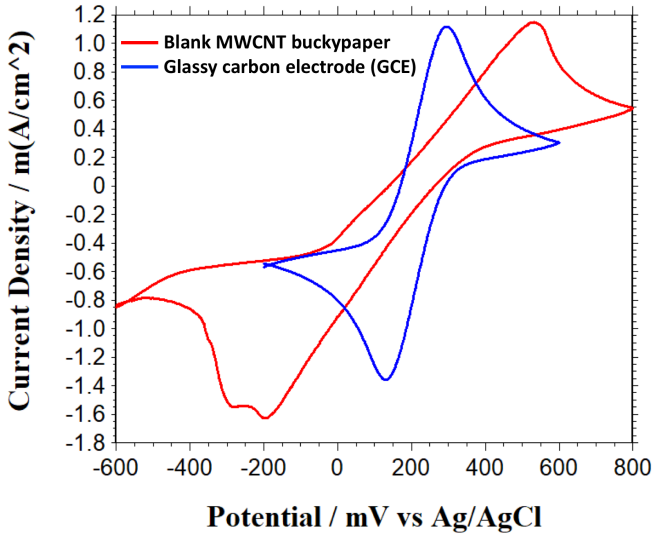

Figure 4.2 *Cyclic voltammograms of blank MWCNT buckypaper and glassy carbon electrode in 0.01 M $K_3[Fe(CN)_6]$, 0.1 M KCl solution at a scan rate of 50 mV s^{-1}*

As previously reported[30, 31], direct electron transfer is an important pathway in the bioelectrochemical systems involving carbon nanomaterials (*e.g.,* MWCNT and graphene) as the electrode. Graphene is a two-dimensional (2D) carbon allotrope composed of sp^2 hybridized carbon atoms and is also the building material for one-dimensional (1D) MWCNT[32, 33]. Reducing graphene oxide to reduced graphene oxide (rGO) is considered as an alternative method to produce graphene in a large scale[33]. More importantly, rGO is more conductive compared with MWCNT[32, 33]. Therefore, the direct electron transfer of fdsABG was tested using MWCNT and rGO modified GCE electrodes, then the electrochemical response of each electrode was measured. Each GCE was drop casted with MWCNT or rGO, and FdsABG were drop casted on each group of electrodes. Cyclic voltammograms (CVs) of these groups electrodes were performed in a CO_2 or N_2-saturated substrate buffered at pH 7.0 with 100 mM K-PO_4. Comparing data from control electrodes (no fdsABG) and from electrodes with fdsABG under conditions with and without substrate CO_2, the CV curves showed all non-turnover signals (Figure 4.3A). Based on the CV data, FdsABG was adsorbed on the electrode surface and became electroactive, however, it did not undergo turnover. This trend suggests that FdsABG was inhibited on the electrodes even in the presence of reaction substrates. This non-turnover signal may result from bad electron communication between electrode and FdsABG. From the non-turnover signal of FdsABG (at pH 7), there is a pair of peaks at approximately -450 mV *vs*. standard Ag/AgCl electrode, which correspond to the reduction and oxidation of the FMN center in fdsABG. Another non-turnover signal from FdsBG showed identical peaks at around -450 mV *vs*. Ag/AgCl (Figure 4.3B), which confirmed that this pair of peaks

were from the FMN center on the ß subunit (FdsB). No response was attributable to the Mo cofactor center, *i.e.*, Mo $^{VI/V}$ or Mo $^{V/IV}$ couple. An oxidation peak at potential -200 mV *vs*. Ag/AgCl could be from the iron-sulfur clusters. These results suggest that the FMN cofactor from fdsB subunit is the easiest accessible cofactor of all. However, the iron-sulfur clusters and Mo center are difficult to access, and this may be because that the cofactors in the complex protein structure are too remote from the electrode surface for direct redox reactions to take place.

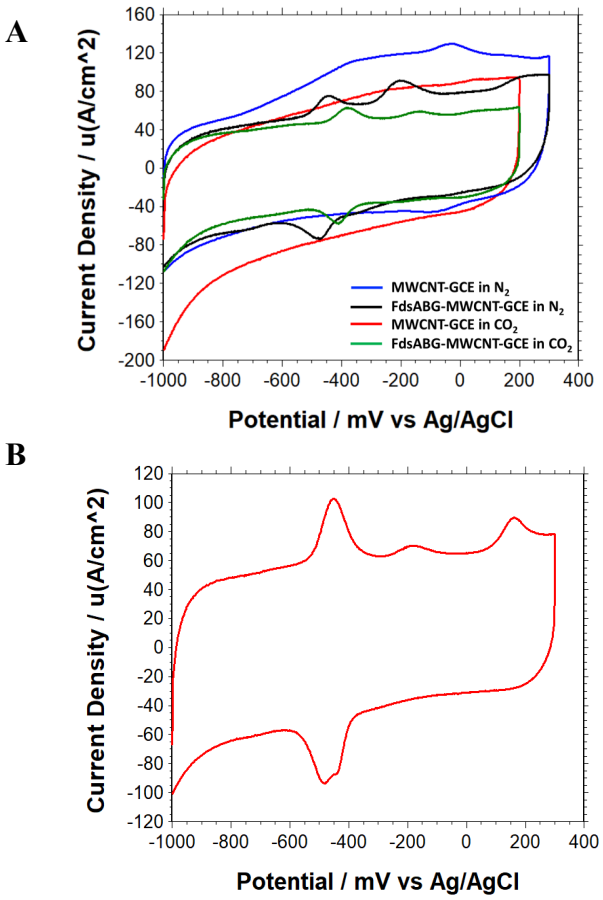

Figure 4.3 *Cyclic voltammograms of non-turnover signals from FdsABG (A) and FdsBG (B) in 0.1 M K-PO₄, 0.1 M KCl solution with/without CO_2 at a scan rate of 10 mV s^{-1}. CVs from MWCNT-GCE electrode in Figure 3A are control experiments.*

Prior studies have reported[11, 12] that a very thin layer (*e.g.*, a monolayer) of enzyme (calculated value $3.5x10^{-12}$ mol cm^{-2}) on the electrode surface is very important for the direct electron transfer in bioelectrochemical systems. This is because too many layers of protein on electrode surface will create an insulating layer between electrons provided by the electrode and reaction substrate in the electrolyte. Accordingly, different mass loadings of fdsABG (0.05-5 μg) were tested on MWCNT-GCE and rGO-GCE electrodes (surface area 0.07 cm^2). The electrochemical response of each electrode was measured under the same condition as experiments shown in Figure 4.3A. However, the CV curves are all non-turnover signals similar to the curves shown in Figure 4.3A. This result has confirmed that iron-sulfur clusters and Mo cofactor are far away from the electrode surface, and electrons from electrode are difficult to flow to the enzyme Mo redox center, which make the DET type bioelectrocatalysis is difficult to achieve.

4.4.2 *C. necator* FdsABG has mediated electron transfer (MET) with electrode

In addition to DET, electrons can be shuttled by small redox species (electron transfer mediator) between enzymes and electrodes. Mediator electron transfer (MET) can not only avoid the problem of random protein orientation on the electrode but can also greatly improve electron transfer rate between enzyme and electrode[16, 23] . Meanwhile, mediators usually have shortcomings including toxicity to the environment, high cost and light sensitivity [34]. Different mediators have different redox potentials ranging from negative to positive values. A potential difference between the mediator and the enzyme

redox cofactor is required for an efficient MET. Equation 4.1 defines the relationship between the Gibbs free energy and the cell potential, where G is the Gibbs free energy, n is the number of electrons, F is the Faraday constant and E_{emf} is the electromotive force between the enzyme cofactor and mediator.

$$\Delta G=-nFE_{emf} \qquad \text{(Eq. 4.1)}$$

From previous non-turnover results of FdsABG, FMN (E_0 = -200 mV vs. SHE) is the most dominant cofactor in FdsABG to communicate with electrode. Also, previous study mentioned that electrons cannot bypass FMN and jump start to iron-sulfur clusters or the Mo cofactor[35]. Therefore, in this study, we employed methyl viologen (MV, E0' = -450 mV vs. SHE) as the mediator to fit in this bioelectrochemistry system, so that it possesses a relative high magnitude of potential difference to the redox potential of FMN.

Since MWCNT-GCE and rGO-GCE have no difference in their response with FdsABG in DET, the MWCNT-GCE composite electrode was selected for subsequent studies due to the easy fabrication process of MWCNT-GCE electrode. Consequently, electrochemical characterizations of MWCNT-GCE electrode were conducted in responses towards the redox reactions of ferricyanide (FCN). Figure 4.4 illustrates cyclic voltammograms (CVs) of the unmodified GCE and MWCNT-GCE electrodes in 0.01 M $K_3[Fe(CN)_6]$, 0.1 M KCl solution at a scan rate of 50 mV s^{-1}. As shown in the figure 4.4, the oxidation and reduction peaks of FCN showed a significant difference in peak-to-peak potential separation on these two groups of electrodes. Furthermore, the peak oxidation

current of FCN from MWCNT-GCE (located at about 0.28 V *vs*. Ag/AgCl) were three orders of magnitude higher than that of the unmodified GCE. The high peak current responses from MWCNT-GCE could be attributed to the enhancements of surface area, electron transfer and the electrocatalytic properties of the MWCNT.

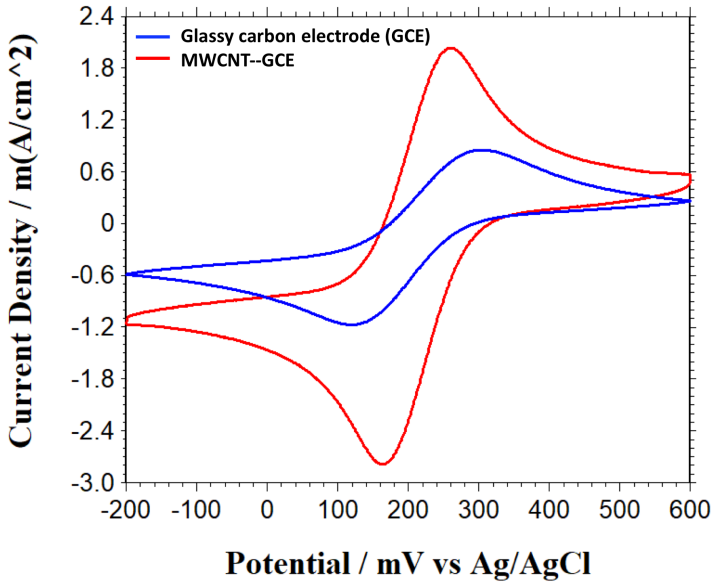

Figure 4.4 *Cyclic voltammograms of blank MWCNT-GCE electrode and glassy carbon electrode (GCE) in 0.01 M $K_3[Fe(CN)_6]$, 0.1 M KCl solution at a scan rate of 50 mV s^{-1}*

Initially, a FdsABG bioelectrode was constructed by adsorbing fdsABG on a GCE electrode that was modified by a mixed solution of MWCNT and chitosan. The resultant bioelectrode was subsequently tested for the bioelectrocatalytic suitability of both CO_2 reduction and formate oxidation in the presence of MV as electron transfer mediator. As shown in Figure 4.5, cyclic voltammograms (CVs) of the fdsABG modified MWCNT-GCE electrodes exhibited catalytic interconversion of formate and CO_2 in 0.1 M K-PO_4 and 0.1 M KCl solution at a scan rate of 10 mV s^{-1}. In absence of either formate or CO_2 as

the substrate, the voltammograms was under non-turnover conditions. The reduction potential (E^0) of the MV redox couple determined to be - 0.65 V *vs.* Ag/AgCl, and the magnitude of potential difference to the redox potential of FMN is approximately 250 mV. With the addition of CO_2 (Figure 4.5A), formate (Figure 4.5B), or both CO_2 and formate as the substrates (Figure 4.5C), catalytic waves were observed. Both catalytic waves of formate oxidation and CO_2 reduction are initiated at about -0.6 V *vs.* Ag/AgCl, and this observed potential was close to the theoretical reduction potential of CO_2 calculated from Nernst equation. [11, 12, 36] Both the rates of formate oxidation and CO_2 reduction increased as the overpotential increased, with the maximal current peaks appearing at above -0.4 V *vs.* Ag/AgCl and below -0.75 V *vs.* Ag/AgCl. The catalytic wave exhibited a sigmoidal shape curve as the overpotential is increased. Meanwhile, there was also an oxidation peak occurring at about -0.5 V *vs*. Ag/AgCl on the catalytic waves of CO_2 reduction, and a reduction peak occurring at about -0.75 V *vs*. Ag/AgCl on the catalytic waves of formate oxidation. This unique peak had a potential from methyl viologen redox couple ($MV^{2+}/MV^{+\bullet}$) at -0.65 V *vs.* Ag/AgCl, and this peak current decreased as the enzyme degraded after several CVs. Therefore, this peak is likely associate with an evidence of an electron transfer step between MV and the enzyme. In detailed explanation, the methyl viologen redox couple ($MV^{2+}/MV^{+\bullet}$) at -0.65 V *vs.* Ag/AgCl generates an electron flow to the FdsABG via FMN, a cofactor on fdsB subunit. Similar electron flow process was found from another Mo containing DMSO reductase from *Rhodobacter sphaeroides* belonging to the same DMSO reductase family of FdsABG[37]. Control experiments were performed using blank MWCNT-GCE electrodes and FdsBG absorbed MWCNT-GCE electrodes

under the same experimental conditions, and no catalytic wave showed (Figure 4.6). These results confirmed that the catalytic wave is from active *C. necator* FdsABG, and FdsABG is able to reversibly convert formate and CO_2 by MV as the electron transfer mediator, which transfer electrons with FdsABG via FMN.

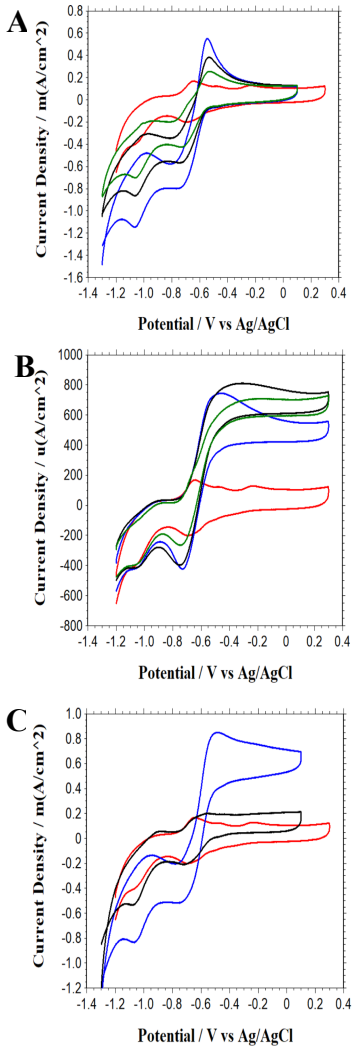

Figure 4.5 *Cyclic voltammograms of catalytic waves from FdsABG in 0.1 M K-PO_4, 0.1 M KCl and 5 mM MV solution with saturated CO_2 only (A), formate only (B) or both saturated CO_2 and formate (C) at a scan rate of 10 mV s^{-1}.*

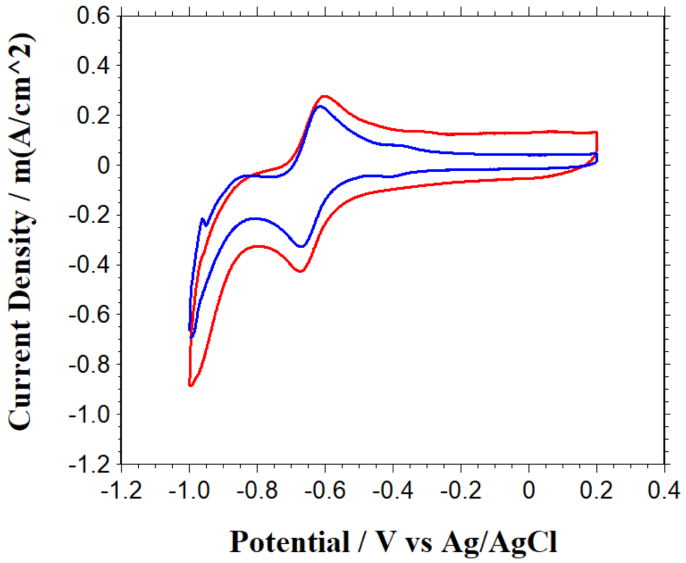

Figure 4.6 *Cyclic voltammograms of FdsABG-MWCNT-GCE and MWCNT-GCE electrodes in 0.1 M K-PO₄, 0.1 M KCl and 5 mM MV solution with saturated CO_2 gas.*

In addition to MV, we have also tested NADH as the electron transfer mediator. Prior studies have shown that FdsABG naturally utilizes NAD^+/NADH as a terminal electron acceptor/donor in enzymatic reactions (Chapter 2) and is able to produce formate from CO_2 by recycling NAD^+ to NADH enzymatically (Chapter 3)[17]. Previous study has shown that a current of NAD^+ reduction was observed at -600 mV vs. Ag/AgCl by using a poly-Neutral Red modified electrode[38, 39]. Here we tried to electrochemically reduce NAD^+ to NADH, and subsequently coupled it with FdsABG to bioelectrochemically catalyze the reduction of CO_2 to formate. Despite the effort, there is no catalytic wave observed from CVs. Additionally, this trend was confirmed by an amperometric i–t curve with potentials applied at -800 mV vs. Ag/AgCl with and without the substrate of CO_2. This observation suggests that NAD^+ is not a fast-redox species from the modified electrode, and FdsABG

could not generate sufficient electrons from the electrochemically reduced NADH for the reaction of CO_2 reduction.

4.4.3 Kinetic results

In this phase of the study, after understanding the reversibility of the reaction by MV as the electron transfer mediator, we determined the kinetic parameters of the FdsABG_MWCNT_GCE electrode by amperometric analysis for the reduction of CO_2. The reductive current of FdsABG_MWCNT_GCE electrode with 5 mM MV was measured with an applied potential at -800 mV vs. Ag/AgCl. The supporting electrolyte started as 0.1 M K-PO_4, 0.1 M KCl, pH 6.5 and saturated with pure N_2 gas at 1 atm. Following that, a CO_2 saturated stock solution (prepared from dissolving CO_2 gas) was successively injected to the electrolyte. The observed reduction current was calibrated to the correct current by Equation 4.2 in order to offset the change in the electrolyte volume, where v is the added volume, V is the initial volume, i_o is the current observed and i_c is the correct current.

$$\frac{(v+V)}{V} i_o = i_c \qquad \text{(Eq. 4.2)}$$

As shown in Figure 4.7, the results yielded increasing reductive currents from the electroenzymatic reduction of CO_2. This reaction can yield a maximum current density of 0.4 mA/cm^2 when the dissolved CO_2 concentration is at its maximum at 1 atm. The observed maximum current density represented to a fast electro catalytic rate of FdsABG. In comparing with other FDHs, *Sf*FDH1 has a maximum current density of 5 µA/cm^2 and *Ec*FDH-H is 80 µA/cm^2 [11, 12]. Although both of those maximum current density were from DET-type bioelectrocatalysis of converting CO_2 to formate, the maximum current density

of MET-type bioelectrocatalysis of FdsABG is still remarkable. In general, MET-type bioelectrocatalysis is always faster than DET-type bioelectrocatalysis.

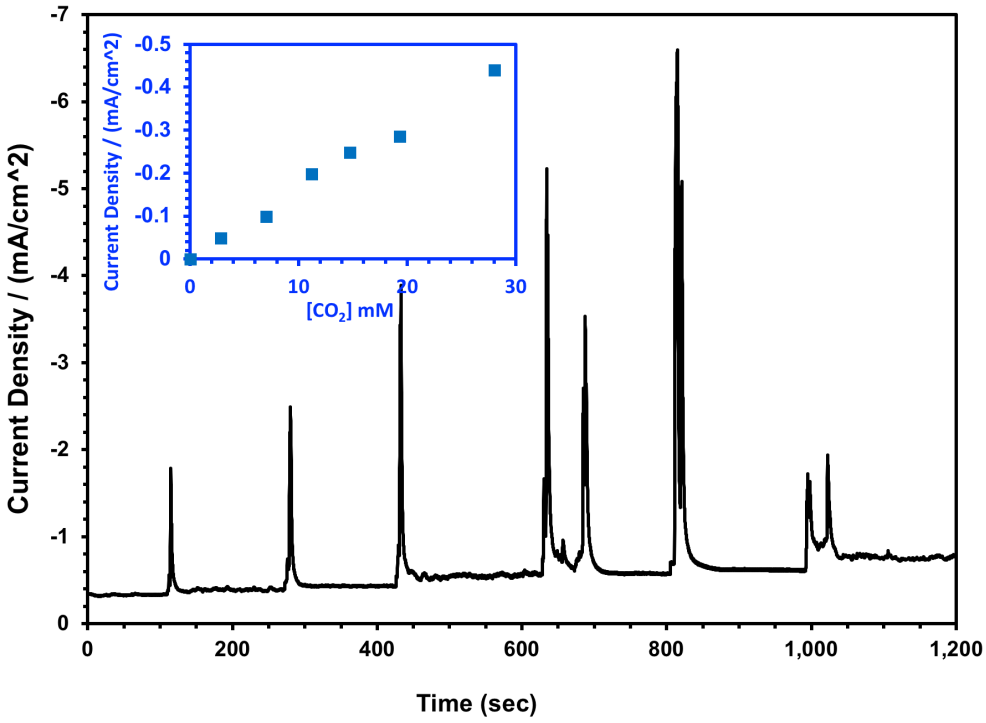

Figure 4.7 *Amperometric analysis (i-t) for the reduction of CO_2 with using FdsABG_MWCNT_GCE electrode at -800 mV vs. Ag/AgCl. The electrolyte started with 0.1 M K-PO_4, 0.1 M KCl, 5 mM MV pH 6.5 and saturated with pure N_2 gas 1 atm, and dissolved CO_2 were injected to the cell subsequently.*

4.4.4 IC confirmation

Finally, we confirmed by ion chromatography that the reaction product of the reduction of CO_2 electrocatalzed by FdsABG was formate. A bulk electrocatalysis was performed for formic acid analysis. In brief, FdsABG_MWCNT_GCE electrode was incubated with an anaerobic and saturated CO_2 solution with 5 mM MV and 20 mM Bis-

Tris propane (final pH 6.3, 25˚C). The reaction was followed by reduction current at -800 mV vs. Ag/AgCl for 2 hours. An aliquot was withdrawn and analyzed by ion chromatography to quantify the concentration of formic acid. Furthermore, the total charge from the bulk electrocatalysis was calculated by integrating the total current with time. This calculation gave the theoretical stoichiometric yield of formic acid using Equations 4.3, 4.4, and 4.5: Faradaic efficiency is calculated from observed coulombs of charge divide by theoretical coulombs of charge (Eq. 4.3). The theoretical charge coulomb is the integration of current over time in experiment (Eq. 4.4). The observed charge coulomb is the formate concentration times 2F (Eq. 4.5), where 2 is for 2 electrons involved in reducing CO_2 to formate, and F s the faradaic constant. Our experiment determined a faradaic efficiency of 96%. These results demonstrate that formate is the only product for the bioelectrocatalysis reaction in the reverse direction.

$$f_{eff} = \frac{Q_e}{Q_t} \quad \text{(Eq. 4.3)}$$

$$Q_e = ixt \quad \text{(Eq. 4.4)}$$

$$Q_t = 2F * [HCOOH] \quad \text{(Eq. 4.5)}$$

4.5 Conclusion

In summary from above studies, *C. necator FdsABG* has no direct electron response to the bioelectrochemical system. This may be associated with the structure complexity of the *C. necator FdsABG.* Specifically, *C. necator FdsABG, Sf*FDH1 and *Ec*FDH-H are all from the DMSO reductase family, which has the most complex Mo active site of all enzymes in

Mo and W superfamily. Different from *Sf*FDH1 and *Ec*FDH-H, *FdsABG* not only has the most complex Mo active site structure, a super large protein size, but also has complex protein cofactors buried inside of the structure, which makes the process of direct electron transfer to the FdsABG a big challenge. Our non-turnover study has shown that FMN from FdsB cofactor is the easiest accessed cofactor in FdsABG to communicate with electrode. Electrons cannot bypass FMN and jumpstart to iron-suffer clusters or the Mo cofactor. Although no catalytic wave was found from DET, the non-turnover results of FdsABG is still very informative, which provides us guidance to identify the optimal electron transfer mediators in the future. In addition, we found that the methyl viologen redox couple ($MV^{2+}/MV^{+\bullet}$) generates an electron flow to FdsABG via FMN, and FdsABG can bioelectrochemically catalyzes the reaction of interconverting CO_2 and formate using Methyl viologen (MV) as the electron transfer mediator. We further studied the kinetic parameters of the FdsABG on electrode for the reduction of CO_2 and confirmed that formate was the only product.

4.6 Reference

1. Appel, A. M.; Bercaw, J. E.; Bocarsly, A. B.; Dobbek, H.; DuBois, D. L.; Dupuis, M.; Ferry, J. G.; Fujita, E.; Hille, R.; Kenis, P. J. A.; Kerfeld, C. A.; Morris, R. H.; Peden, C. H. F.; Portis, A. R.; Ragsdale, S. W.; Rauchfuss, T. B.; Reek, J. N. H.; Seefeldt, L. C.; Thauer, R. K.; Waldrop, G. L., Frontiers, Opportunities, and Challenges in Biochemical and Chemical Catalysis of CO_2 Fixation. Chemical Reviews 2013, 113 (8), 6621-6658.

2. Aresta, M.; Dibenedetto, A.; Angelini, A., Catalysis for the Valorization of Exhaust Carbon: from CO_2 to Chemicals, Materials, and Fuels. Technological Use of CO_2. Chemical Reviews 2014, 114 (3), 1709-1742.

3. Maia, L. B.; Moura, I.; Moura, J. J. G., Molybdenum and tungsten-containing formate dehydrogenases: Aiming to inspire a catalyst for carbon dioxide utilization. Inorganica Chimica Acta 2017, 455, 350-363.

4. Enthaler, S.; von Langermann, J.; Schmidt, T., Carbon dioxide and formic acid-the couple for environmental-friendly hydrogen storage? Energy & Environmental Science 2010, 3 (9), 1207-1217.

5. Sordakis, K.; Tang, C. H.; Vogt, L. K.; Junge, H.; Dyson, P. J.; Beller, M.; Laurenczy, G., Homogeneous Catalysis for Sustainable Hydrogen Storage in Formic Acid and Alcohols. Chemical Reviews 2018, 118 (2), 372-433.

6. Yadav, M.; Xu, Q., Liquid-phase chemical hydrogen storage materials. Energy & Environmental Science 2012, 5 (12), 9698-9725.

7. Preuster, P.; Albert, J., Biogenic Formic Acid as a Green Hydrogen Carrier. Energy Technology 2018, 6 (3), 501-509.

8. Aresta, M.; Dibenedetto, A., Utilisation of CO_2 as a chemical feedstock: opportunities and challenges. Dalton Transactions 2007, (28), 2975-2992.

9. Shi, J. F.; Jiang, Y. J.; Jiang, Z. Y.; Wang, X. Y.; Wang, X. L.; Zhang, S. H.; Han, P. P.; Yang, C., Enzymatic conversion of carbon dioxide. Chemical Society Reviews 2015, 44 (17), 5981-6000.

10. Srikanth, S.; Maesen, M.; Dominguez-Benetton, X.; Vanbroekhoven, K.; Pant, D., Enzymatic electrosynthesis of formate through CO_2 sequestration/reduction in a bioelectrochemical system (BES). Bioresource Technology 2014, 165, 350-354.

11. Reda, T.; Plugge, C. M.; Abram, N. J.; Hirst, J., Reversible interconversion of carbon dioxide and formate by an electroactive enzyme. Proceedings of the National Academy of Sciences of the United States of America 2008, 105 (31), 10654-10658.

12. Bassegoda, A.; Madden, C.; Wakerley, D. W.; Reisner, E.; Hirst, J., Reversible lnterconversion of CO_2 and Formate by a Molybdenum-Containing Formate Dehydrogenase. Journal of the American Chemical Society 2014, 136 (44), 15473-15476.

13. de Bok, F. A. M.; Hagedoorn, P. L.; Silva, P. J.; Hagen, W. R.; Schiltz, E.; Fritsche, K.; Stams, A. J. M., Two W-containing formate dehydrogenases (CO_2-reductases) involved in syntrophic propionate oxidation by *Syntrophobacter fumaroxidans*. European Journal of Biochemistry 2003, 270 (11), 2476-2485.

14. Boyington, J. C.; Gladyshev, V. N.; Khangulov, S. V.; Stadtman, T. C.; Sun, P. D., Crystal structure of formate dehydrogenase H: Catalysis involving Mo, molybdopterin, selenocysteine, and an Fe_4S_4 cluster. Science 1997, 275 (5304), 1305-1308.

15. Zinoni, F.; Birkmann, A.; Stadtman, T. C.; Bock, A., Nucleotide sequence and expression of the selenocysteine-containing polypeptide of formate dehydrogenase (formate-hydrogen-lyase-linked) from *Escherichia coli*. Proceedings of the National Academy of Sciences of the United States of America 1986, 83 (13), 4650-4654.

16. Kalimuthu, P.; Bernhardt, P. V., Electrochemistry of Molybdenum and Tungsten Enzymes. Molybdenum and Tungsten Enzymes: Spectroscopic and Theoretical Investigations 2017, 7, 168-222.

17. Yu, X. J.; Niks, D.; Mulchandani, A.; Hille, R., Efficient reduction of CO_2 by the molybdenum-containing formate dehydrogenase from *Cupriavidus necator* (*Ralstonia eutropha*). Journal of Biological Chemistry 2017, 292 (41), 16872-16879.

18. Oh, J. I.; Bowien, B., Structural analysis of the fds operon encoding the NAD(+)-linked formate dehydrogenase of *Ralstonia eutropha*. Journal of Biological Chemistry 1998, 273 (41), 26349-26360.

19. Niks, D.; Duvvuru, J.; Escalona, M.; Hille, R., Spectroscopic and Kinetic Properties of the Molybdenum-containing, NAD(+) - dependent Formate Dehydrogenase from *Ralstonia eutropha*. Journal of Biological Chemistry 2016, 291 (3), 1162-1174.

20. Hille, R.; Hall, J.; Basu, P., The Mononuclear Molybdenum Enzymes. Chemical Reviews 2014, 114 (7), 3963-4038.

21. Weckbecker, A.; Groeger, H.; Hummel, W., Regeneration of Nicotinamide Coenzymes: Principles and Applications for the Synthesis of Chiral Compounds. Biosystems Engineering I: Creating Superior Biocatalysts 2010, 120, 195-242.

22. Gross, A. J.; Chen, X. H.; Giroud, F.; Abreu, C.; Le Goff, A.; Holzinger, M.; Cosnier, S., A High Power Buckypaper Biofuel Cell: Exploiting 1,10-Phenanthroline-5,6-dione with FAD-Dependent Dehydrogenase for Catalytically-Powerful Glucose Oxidation. Acs Catalysis 2017, 7 (7), 4408-4416.

23. Milton, R. D.; Minteer, S. D., Direct enzymatic bioelectrocatalysis: differentiating between myth and reality. Journal of the Royal Society Interface 2017, 14 (131), 13.

24. Bollella, P.; Gorton, L.; Antiochia, R., Direct Electron Transfer of Dehydrogenases for Development of 3rd Generation Biosensors and Enzymatic Fuel Cells. Sensors (Basel, Switzerland) 2018, 18 (5).

25. Xu, S.; Minteer, S. D., Investigating the Impact of Multi-Heme Pyrroloquinoline Quinone-Aldehyde Dehydrogenase Orientation on Direct Bioelectrocatalysis via Site Specific Enzyme Immobilization. Acs Catalysis 2013, 3 (8), 1756-1763.

26. Baughman, R. H.; Zakhidov, A. A.; de Heer, W. A., Carbon nanotubes - the route toward applications. Science 2002, 297 (5582), 787-792.

27. Zhu, H. W.; Wei, B. Q., Assembly and applications of carbon nanotube thin films. Journal of Materials Science & Technology 2008, 24 (4), 447-456.

28. Grosse, W.; Champavert, J.; Gambhir, S.; Wallace, G. G.; Moulton, S. E., Aqueous dispersions of reduced graphene oxide and multi wall carbon nanotubes for enhanced glucose oxidase bioelectrode performance. Carbon 2013, 61, 467-475.

29. Trojanowicz, M.; Mulchandani, A.; Mascini, M., Carbon nanotubes-modified screen-printed electrodes for chemical sensors and biosensors. Analytical Letters 2004, 37 (15), 3185-3204.

30. Terse-Thakoor, T.; Komori, K.; Ramnani, P.; Lee, I.; Muchandani, A., Electrochemically Functionalized Seamless Three-Dimensional Graphene-Carbon Nanotube Hybrid for Direct Electron Transfer of Glucose Oxidase and Bioelectrocatalysis. Langmuir 2015, 31 (47), 13054-13061.

31. Freire, R. S.; Pessoa, C. A.; Mello, L. D.; Kubota, L. T., Direct electron transfer: An approach for electrochemical biosensors with higher selectivity and sensitivity. Journal of the Brazilian Chemical Society 2003, 14 (2), 230-243.

32. Xu, M. S.; Liang, T.; Shi, M. M.; Chen, H. Z., Graphene-Like Two-Dimensional Materials. Chemical Reviews 2013, 113 (5), 3766-3798.

33. Zhu, Y. W.; Murali, S.; Cai, W. W.; Li, X. S.; Suk, J. W.; Potts, J. R.; Ruoff, R. S., Graphene and Graphene Oxide: Synthesis, Properties, and Applications. Advanced Materials 2010, 22 (35), 3906-3924.

34. Chaubey, A.; Malhotra, B. D., Mediated biosensors. Biosensors & Bioelectronics 2002, 17 (6-7), 441-456.

35. Kalimuthu, P.; Ringel, P.; Kruse, T.; Bernhardt, P. V., Direct electrochemistry of nitrate reductase from the fungus *Neurospora crassa*. Biochimica Et Biophysica Acta-Bioenergetics 2016, 1857 (9), 1506-1513.

36. Armstrong, F. A.; Hirst, J., Reversibility and efficiency in electrocatalytic energy conversion and lessons from enzymes. Proceedings of the National Academy of Sciences of the United States of America 2011, 108 (34), 14049-14054.

37. Abo, M.; Ogasawara, Y.; Tanaka, Y.; Okubo, A.; Yamazaki, S., Amperometric dimethyl sulfoxide sensor using dimethyl sulfoxide reductase from *Rhodobacter sphaeroides*. Biosensors & Bioelectronics 2003, 18 (5-6), 735-739.

38. Addo, P. K.; Arechederra, R. L.; Waheed, A.; Shoemaker, J. D.; Sly, W. S.; Minteer, S. D., Methanol Production via Bioelectrocatalytic Reduction of Carbon Dioxide: Role of Carbonic Anhydrase in Improving Electrode Performance. Electrochemical and Solid State Letters 2011, 14 (4), E9-E13.

39. Karyakin, A. A.; Bobrova, O. A.; Karyakina, E. E., Electroreduction of NAD(+) to enzymatically active NADH at poly(neutral red) modified electrodes. Journal of Electroanalytical Chemistry 1995, 399 (1-2), 179-184.

Chapter 5

Conclusions

5.1 Summary

My dissertation research aims to investigate a high-efficiency and cost-effective bioelectrocatalytic process for transformation of the abundant waste carbon dioxide to formic acid, a useful chemical fuel and feedstock, by the novel soluble and oxygen tolerant formate dehydrogenase (FdsABG) from *Cupriavidus necator* (formerly known as *Ralstonia eutropha*). Before my dissertation research, FdsABG has only been purified from its native bacterium *C. necator* [1-3] and has been reported not able to catalyze the reverse reaction, *i.e.* converting carbon dioxide to formic acid[1,3]. Thus, we did many works to achieve my dissertation goal.

First of all, in chapter 2, we have found that the FdsABG purified from *C. necator* is indeed able to effectively catalyze the reduction of CO_2 using NADH as reductant, stoichiometrically generating formate (as confirmed by NMR) with a $k_{cat}^{CO_2}$ of 10 s^{-1} [4]. Importantly, we demonstrate that the enzyme's steady-state kinetic parameters in the forward and reverse reactions are consistent with the overall thermodynamics of the reaction. Finally, we establish the reaction conditions necessary to quantify the reverse reaction. In conjunction with our earlier studies on the reaction mechanism of this enzyme[2], and on the basis of the present work we conclude that all molybdenum- and tungsten-containing formate dehydrogenases and related enzymes likely operate via a simple

hydride transfer mechanism and are effective in catalyzing the reversible interconversion of CO_2 and formate under the appropriate experimental conditions.

After the work from chapter 2, we were very exciting to the results, including FdsABG is able to catalyze the reaction of converting CO_2 to formate. However, the entire process is highly time consuming and very expensive, not only for protein purification, but also for NADH cofactor. Thus, in chapter 3, we have cloned the full-length soluble formate dehydrogenase (FdsABG) from *C. necator* and expressed in *E. coli* with a 6xHis-linker-6xHis-tag fused to the N terminus of fdsG subunit, and this overexpression system has simplified the FdsABG purification steps from 5-day work to 1-day work compared to protein purification process from native bacteria *C. necator*. We have also combined this engineered *C. necator* FdsABG with another biological enzyme, Glucose Dehydrogenase, for continuous electrons donation to the reaction of converting CO_2 to formate. The results turn out that our engineered *C. necator* FdsABG has a highly thermodynamic efficient to the reduction of CO_2 process with a NADH total turnover number of 1.9.

Last but not least, in chapter 4, we have studied dynamic electrochemistry of the FdsABG from *C. necator*. Unfortunately, we find that *C. necator* FdsABG has no direct electron response to the bioelectrochemical system. This may be associated with the complex structure of the *C. necator* FdsABG, which makes the process of direct electron transfer to the FdsABG a big challenge. Our non-turnover study has shown that FMN from FdsB cofactor is the easiest access cofactor in FdsABG to communicate with electrode. Electrons cannot bypass FMN and jumpstart to iron-suffer clusters or the Mo cofactor. Although no catalytic wave was found from DET, the non-turnover results of FdsABG is

still very informative, which provides us guidance to identify the optimal electron transfer mediators in the future. In addition, we found that the methyl viologen redox couple (MV2+/MV+•) generates an electron flow to FdsABG via FMN, and FdsABG can bioelectrochemically catalyzes the reaction of interconverting CO_2 and formate using Methyl viologen (MV) as the electron transfer mediator. We further studied the kinetic parameters of the FdsABG on electrode for the reduction of CO_2 and confirmed that formate was the only product.

5.2 Suggestions for future work

The interdisciplinary research can provide fundamental knowledge to develop a highly efficient bio-electro-catalytic process for transformation of the greenhouse gas carbon dioxide to formic acid that can be used to power fuel-cells or synthesis of other value-added chemicals. Many works still could be done on fdsABG to improve the efficiency of converting CO_2 to formate.

First of all, fdsABG is converting formate to CO_2 in nature. It has higher binding affinity to formate other than CO_2. Therefore, when producing formate from CO_2, too much formate can inhibit the enzyme activity. We have seen this effect from chapter 3. Thus, in order to continuously produce formate from CO_2 under fdsABG catalysis, the resulting formate need to be continuously removed from the reaction. A flow cell could be possible to solve this problem. In addition, in order to improve the catalytic efficiency and enzyme recycling, enzyme scaffolding and enzyme immobilization can solve such problems.

For bioelectrocatalysis, it is not a good idea to immobilize such a large and complex protein on electrode. The CO_2 catalytic site of FdsABG is on FdsA subunit. If we can truncate the large FdsABG into FdsA or even part of FdsA, the electron transfer process between electrode and enzyme could be much easier and faster than the full length FdsABG. It is anticipated that the catalytic rate of CO_2 reduction will also be greatly increased. We have tried to clone and overexpress FdsA in *E. coli* using the same method of cloning full length FdsABG, but the results were not optimistic. No FdsA was able to express and purify from *E. coli*. A potential future work would be cloning truncated FdsA, which is only leave one Mo center and one iron-sulfur cluster from FdsA. Despite the uncertainties of molecular cloning and protein engineer, this will be an interesting potential work.

5.3 Reference

1. Friedebold, J.; Bowien, B., Physiological and biochemical characterization of the soluble formate dehydrogenase, a molybdoenzyme from *Alcaligenes eutrophus*. Journal of Bacteriology 1993, 175 (15), 4719-4728.

2. Niks, D.; Duvvuru, J.; Escalona, M.; Hille, R., Spectroscopic and Kinetic Properties of the Molybdenum-containing, NAD(+) - dependent Formate Dehydrogenase from *Ralstonia eutropha*. Journal of Biological Chemistry 2016, 291 (3), 1162-1174.

3. Oh, J. I.; Bowien, B., Structural analysis of the fds operon encoding the NAD(+)-linked formate dehydrogenase of *Ralstonia eutropha*. Journal of Biological Chemistry 1998, 273 (41), 26349-26360.

4. Yu, X. J.; Niks, D.; Mulchandani, A.; Hille, R., Efficient reduction of CO_2 by the molybdenum-containing formate dehydrogenase from *Cupriavidus necator* (*Ralstonia eutropha*). Journal of Biological Chemistry 2017, 292 (41), 16872-16879.